

Phenomena in the kink-antikink Collisions of ϕ^8 Theory

Yun Feng^a Yunguo Jiang^{b,1}

^a*SDU-ANU Joint Science College, Shandong University, Weihai, 264209, People's Republic of China*

^b*Shandong Provincial Key Laboratory of Optical Astronomy and Solar-Terrestrial Environment, Institute of Space Sciences, Shandong University, Weihai, 264209, People's Republic of China;*

E-mail: 202200700090@mail.sdu.edu.cn, jiangyg@sdu.edu.cn

ABSTRACT: We investigated kink-antikink collisions in a $(1+1)$ -dimensional ϕ^8 scalar field theory with multiple degenerate vacua. We presented explicit soliton solutions for different vacuum structures characterized by the ratio $n = p_2/p_1$. We focused on the cases $n = 2$ and $n = 3$ with four distinct vacua, and performed systematic numerical simulations across all topological sectors. We revealed that there is a complete annihilation regime in the $(-1/2, 1/2)$ sector, where kink-antikink pairs annihilate for all initial velocities. Up to our knowledge, such phenomenon is first reported in the kink antikink collisions. We revealed a comprehensive fractal cartography of multi-bounce resonance windows across sectors $(-1, -1/2)$, $(-1, -1/3)$, and $(-1/3, 1/3)$. Given the kink antikink ($K\bar{K}$, or $\bar{K}K$) ordering, the effective potential and the spectrum of the Schrödinger like equation were presented. By collecting all the effective potential and collision phenomena, we proposed that the effective potential classification scheme provides a predictive framework for collision outcomes including escape, bion formation, sector change, and annihilation. Especially, it is identified that, when soliton pairs pass through each other, the abrupt changes of the potential type could explain both the sector-change and annihilation phenomena. Our work highlight novel dynamical features of the ϕ^8 model absent in lower-order field theories, and establish connections between topological structure, vibrational modes, and effective potentials.

KEYWORDS: Solitons Monopoles and Instanton, Field Theories in Lower Dimensions

¹Corresponding author: jiangyg@sdu.edu.cn

Contents

1	The introduction of kink dynamics	2
2	The ϕ^8 theory	3
2.1	$n = p_2/p_1 = 2$	5
2.2	$n = p_2/p_1 = 3$	5
2.3	Other n	6
3	The kink-antikink collision in the ϕ^8 Theory	7
3.1	Setup for $\phi_{K\bar{K}}$	8
3.2	Set up of the boundary conditions	10
4	Numerical results	12
4.1	The numerical illustration of collisions	12
4.2	The rich collision phenomena for different topological sector	21
4.3	Unified picture	30
5	Conclusion	31

1 The introduction of kink dynamics

Solitons, also known as solitary waves, are a special type of structure that exist extensively in nonlinear wave equations. Kink is (1+1) dimensional soliton [1]. Kink dynamics is not merely a theoretical mathematical construct and it finds practical applications in multiple physical fields, such as Condensed Matter Physics, Particle Physics, Nonlinear Optics, Biophysics and so on [2, 3, 4, 5].

The study of localized, particle-like solutions in nonlinear field theories, known as solitons, has been a cornerstone of theoretical physics for decades. In (1+1) dimensions, kink solitons—topological defects connecting disparate vacua of a scalar field—serve as a powerful theoretical laboratory for probing fundamental nonlinear phenomena. Among the canonical models, the ϕ^4 theory has been instrumental in elucidating complex dynamical processes. Extensive research has revealed a rich phenomenology, including the formation of bound states (bions), the existence of a critical velocity separating capture from escape, and a characteristic fractal structure of resonance windows in the velocity-impact parameter space [6]. To approximate these intricate dynamics analytically, the collective coordinate (or covariant coordinate) method has emerged as a leading effective approach. This method, which treats the kink’s position as a dynamical variable, has successfully captured the resonant energy exchange mechanism between translational kinetic energy and internal vibrational modes, accurately predicting the locations of resonance windows and critical velocities in ϕ^4 theory [7, 8, 9]. Similar investigations have extended these findings to the ϕ^6 model, revealing parallel yet distinct dynamical features [7].

While the physics of lower-order polynomial models is well-established, the frontier of soliton dynamics is increasingly moving toward more complex potentials. The ϕ^8 theory, characterized by an eighth-degree polynomial potential, represents a particularly compelling and challenging system. Unlike its simpler counterparts, the ϕ^8 potential supports four degenerate vacua, enabling a richer taxonomy of kinks—including elementary and nested configurations—and more intricate interaction landscapes. This complexity makes it an ideal candidate for exploring phenomena that are inaccessible in simpler models. Moreover, although collective coordinate method successfully forecasts the bounce windows, the strong nonlinearity of the ϕ^8 system causes it to break down. Recent studies have begun to unravel its unique properties, from the excitation spectra of kinks with exponential asymptotics [10] to the scattering dynamics of kinks exhibiting power-law asymptotics [11]. A crucial insight from this work is the discovery of a collective vibrational mode supported by the kink-antikink pair as a composite system. Even in the absence of an individual soliton shape mode, this pair-dependent mode facilitates energy transfer during collisions, a mechanism reminiscent of the resonance observed in the ϕ^6 theory [9]. Furthermore, progress has been made in constructing both implicit and explicit kink solutions under specific parameter regimes [12], and in applying robust numerical techniques like the pseudospectral method to solve the challenging boundary value problems associated with these solitons [13]. While recent studies have begun to explore the ϕ^8 model [12], long-term collision dynamics across a wide parameter space—especially the emergent fractal structures, are still not fully understood.

Despite these significant advances, a profound and conspicuous gap in our understanding persists. The majority of previous research has focused on individual soliton properties or two-body scattering at specific energies. A systematic, large-scale investigation into the global, long-term dynamics of kink-antikink collisions in the ϕ^8 model—particularly the emergent fractal structures as a function of both initial velocity and potential shape parameters—is conspicuously absent. This paper is dedicated to filling this critical void. Building upon the methodological foundations laid by previous work, we conduct a comprehensive numerical study of kink-antikink collisions across a wide range of potential field parameters within the ϕ^8 theory. Our primary goal is to map the complex landscape of dynamical outcomes, meticulously categorizing the observed fractal structures and resonance phenomena. By doing so, we aim to not only extend the current knowledge of the ϕ^8 model but also to provide deeper insights into the universal principles governing soliton interactions in higher-order nonlinear field theories.

The remainder of this paper is structured as follows. Section 1 is introduction of kink. Section 2 introduces the ϕ^8 model, detailing both the implicit soliton solutions and the explicit forms derived under special conditions. Section 3 aims to work out boundary conditions. Section 4 outlines the numerical methods employed and presents a detailed analysis of our simulation results, focusing on the fractal structures and dynamical phenomena observed for different parameter sets. Finally, Section 5 summarizes our findings and discusses their implications.

2 The ϕ^8 theory

Considering the (1 + 1) dimension scalar field $\phi(x, t)$, the Lagrangian density can be denoted by [14]

$$\mathcal{L} = \frac{1}{2} \partial_\mu \phi \partial^\mu \phi - V(\phi), \quad (2-1)$$

where $V(\phi)$ is the potential, which can be depicted in different types for different theories. Considering the ϕ^8 theory, its potential $V(\phi)$ can be denoted by

$$V(\phi) = \frac{1}{2} (\phi^2 - p_1^2)^2 (\phi^2 - p_2^2)^2, \quad (p_1 < p_2) \quad (2-2)$$

where p_1 and p_2 are vacuum. There are four vacuum solutions, i.e., $\phi = -p_2, -p_1, p_1,$ and p_2 . Its form of Euler-Lagrange equation is

$$\partial_\mu \partial^\mu \phi + \frac{dV}{d\phi} = 0. \quad (2-3)$$

Ignoring the kinetic term, the total energy of the system can be given by

$$E_{\text{static}}[\phi] = E_{\text{BPS}}[\phi] + \frac{1}{2} \int \left(\frac{d\phi}{dx} \pm \frac{dW}{d\phi} \right)^2 dx, \quad (2-4)$$

where $E_{\text{BPS}} = W[\phi(+\infty)] - W[\phi(-\infty)]$ is the bounded energy and the mass term for the kink and antikink configurations, and $W(\phi)$ is the super potential. For ϕ^8 theory, the

super-potential can be denoted by

$$W(\phi) = \frac{1}{5}\phi^5 - (p_1^2 + p_2^2)\phi^3 + p_1^2 p_2^2 \phi. \quad (2-5)$$

The Bogomolynyi-Prasad-Sommerfield (BPS) equation [15] is obtained by minimizing the total energy, which reads

$$\frac{d\phi}{dx} = \pm \frac{dW}{d\phi}. \quad (2-6)$$

It is a first-order equation which can be used to work out the specific form of kink solutions. All the masses of kinks and antikinks [12] can be denoted by

$$M(p_1, p_2) = M(-p_2, -p_1) = \frac{2(p_2 - p_1)^3(p_1^3 + 3p_1 p_2 + p_2^3)}{15}, \quad (2-7)$$

$$M(-p_1, p_1) = \frac{4p_1^3(5p_2^2 - p_1^2)}{15}.$$

The kink solutions of the ϕ^8 theory can be worked out by the BPS equation, and they interpolate between the adjacent vacuums. There are six kink solutions in the ϕ^8 theory. Because of the intricate high-level nonlinear potential field, there is no universal explicit solution. When p_2/p_1 takes some unique values, there are explicit solutions ($\phi = \phi(x)$) for the ϕ^8 theory. These explicit potentials are presented in Figure 1.

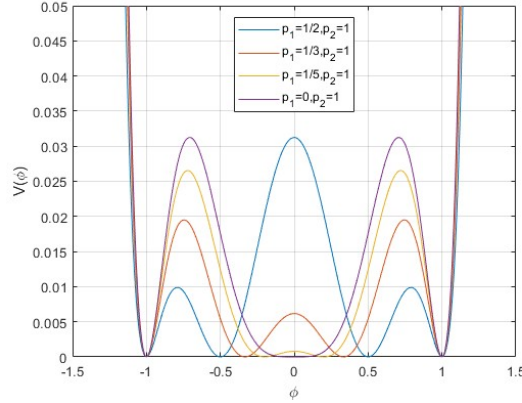


Figure 1: Different potentials in the ϕ^8 theory

There are still some implicit kink solutions. First, we consider the Topological sectors (p_1, p_2) and $(-p_2, -p_1)$. By integrating the BPS equation under the condition $0 < a < |\phi| < b$, we can obtain an implicit solution [12]

$$x = \frac{1}{2(p_2^2 - p_1^2)} \ln \left[\left(\frac{\phi - p_1}{\phi + p_1} \right)^{\frac{1}{p_1}} \left(\frac{p_2 + \phi}{p_2 - \phi} \right)^{\frac{1}{p_2}} \right]. \quad (2-8)$$

And Equation 2-8 can be transformed into

$$\left(\frac{\phi - p_1}{\phi + p_1} \right)^{\frac{p_2}{p_1}} \left(\frac{p_2 + \phi}{p_2 - \phi} \right) = \exp [2p_2(p_2^2 - p_1^2)x]. \quad (2-9)$$

Then denoting $p_2/p_1 = n$ and setting $p_2 = 1$, Equation 2-9 becomes

$$\left(\frac{n\phi - 1}{n\phi + 1}\right)^n \left(\frac{1 + \phi}{1 - \phi}\right) = \exp \left[2 \left(1 - \frac{1}{n^2}\right) x \right]. \quad (2-10)$$

We will present the solution for different n values below.

2.1 $n = p_2/p_1 = 2$

When $n = 2$, by solving the Equation 2-10, the kink solutions can be described by the universal form

$$\phi_m(x) = \cos \left\{ \frac{1}{3} \arccos \left[\tanh\left(\frac{3}{4}x\right) \right] + \frac{\pi}{3}m \right\}, \quad (2-11)$$

where $m = 0, 1, 2, 3, 4, 5$. In this formula, the subscript m of ϕ illustrates the different types of kinks. As a prime instance, $m = 1$ represents that kink is between the vacuums $\phi(-\infty) = -p_1$ and $\phi(+\infty) = p_1$. There are six different types of kinks which are plotted in the Figure 2. The corresponding soliton mass can be derived from Equation 2-7, i.e.,

$$M_{(\frac{1}{2},1)} = M_{(-1,-\frac{1}{2})} = \frac{11}{240}, \quad M_{(-\frac{1}{2},\frac{1}{2})} = \frac{19}{240}. \quad (2-12)$$

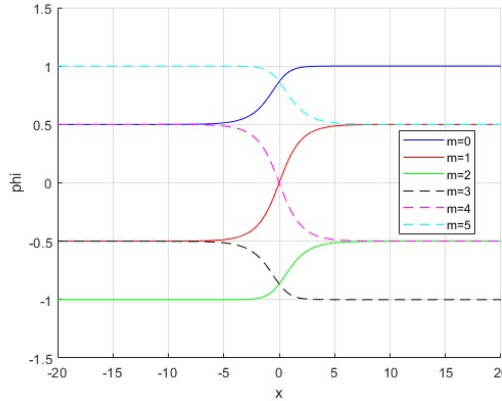


Figure 2: Kinks and antikinks when $n = 2$ in the ϕ^8 theory for $p_1 = 0.5$ and $p_2 = 1$.

2.2 $n = p_2/p_1 = 3$

When $n = 3$ ($p_2 = 1$ and $p_1 = 1/3$), the kink solutions can be given in three intervals. For the sector $(-1, -1/3)$, the kink solution reads

$$\phi_K(x) = \begin{cases} \frac{1}{3} \left[-\sqrt{1 - (\sec \frac{8}{9}x)^{\frac{2}{3}}} - \sqrt{2 + (\sec \frac{8}{9}x)^{\frac{2}{3}}} - \frac{2 \tanh \frac{8}{9}x}{\sqrt{1 - (\sec \frac{8}{9}x)^{\frac{2}{3}}}} \right], & x < 0. \\ \frac{1}{3} \left[\sqrt{1 - (\sec \frac{8}{9}x)^{\frac{2}{3}}} - \sqrt{2 + (\sec \frac{8}{9}x)^{\frac{2}{3}}} + \frac{2 \tanh \frac{8}{9}x}{\sqrt{1 - (\sec \frac{8}{9}x)^{\frac{2}{3}}}} \right], & x > 0. \end{cases} \quad (2-13)$$

And it satisfies the limitation

$$\lim_{x \rightarrow -0} \phi_K(x) = \lim_{x \rightarrow +0} \phi_K(x) = -\frac{\sqrt{3+2\sqrt{3}}}{3}. \quad (2-14)$$

For the sector $(1/3, 1)$, the kink solution reads

$$\phi_K(x) = \begin{cases} \frac{1}{3} \left[-\sqrt{1 - (\sec \frac{8}{9}x)^{\frac{2}{3}}} + \sqrt{2 + (\sec \frac{8}{9}x)^{\frac{2}{3}} - \frac{2 \tanh \frac{8}{9}x}{\sqrt{1 - (\sec \frac{8}{9}x)^{\frac{2}{3}}}}} \right], & x < 0 \\ \frac{1}{3} \left[\sqrt{1 - (\sec \frac{8}{9}x)^{\frac{2}{3}}} + \sqrt{2 + (\sec \frac{8}{9}x)^{\frac{2}{3}} + \frac{2 \tanh \frac{8}{9}x}{\sqrt{1 - (\sec \frac{8}{9}x)^{\frac{2}{3}}}}} \right], & x > 0. \end{cases} \quad (2-15)$$

And it satisfies the limitation

$$\lim_{x \rightarrow -0} \phi_K(x) = \lim_{x \rightarrow +0} \phi_K(x) = \frac{\sqrt{3+2\sqrt{3}}}{3}. \quad (2-16)$$

For sector $(-1/3, 1/3)$, the kink solution reads

$$\phi_K(x) = \begin{cases} \frac{1}{3} \left[\sqrt{1 + (\csc \frac{8}{9}x)^{\frac{2}{3}}} - \sqrt{2 - (\csc \frac{8}{9}x)^{\frac{2}{3}} - \frac{2 \coth \frac{8}{9}x}{\sqrt{1 + (\csc \frac{8}{9}x)^{\frac{2}{3}}}}} \right], & x < 0 \\ \frac{1}{3} \left[-\sqrt{1 + (\csc \frac{8}{9}x)^{\frac{2}{3}}} + \sqrt{2 - (\csc \frac{8}{9}x)^{\frac{2}{3}} + \frac{2 \coth \frac{8}{9}x}{\sqrt{1 + (\csc \frac{8}{9}x)^{\frac{2}{3}}}}} \right], & x > 0. \end{cases} \quad (2-17)$$

And it satisfies the limitation

$$\lim_{x \rightarrow -0} \phi_K(x) = \lim_{x \rightarrow +0} \phi_K(x) = 0. \quad (2-18)$$

The anti-kink solution $\phi_{\bar{K}}$ could be obtained by replacing $x \rightarrow -x$ in ϕ_K . The corresponding kink mass can be derived from Equations 2-7

$$M_{(\frac{1}{3}, 1)} = M_{(-1, -\frac{1}{3})} = \frac{304}{3645}, \quad M_{(-\frac{1}{3}, \frac{1}{3})} = \frac{176}{3645}. \quad (2-19)$$

These three types of kinks are depicted in the Figure 3.

Based on the explicit formula of the $n = 2$ and $n = 3$ kinks, we can speculate that if there are explicit kink solutions in higher n , they will be more complicated.

2.3 Other n

According to the kink solution ϕ^8 theory [12], when n is a rational value, its asymptotics of kink solutions should be discussed for different sectors. We consider the asymmetric kink $(-1/n, 1)$ and symmetric kink $(-1/n, 1/n)$ which are given below

(i) **asymmetric kink** $(-1/n, 1)$

$$\phi_K(x) = \frac{1}{n} + \frac{2}{n} \left(\frac{n-1}{n+1} \right)^{1/n} \exp \left[\frac{2}{n} \left(1 - \frac{1}{n^2} \right) x \right], \quad \text{when } x \rightarrow -\infty. \quad (2-20)$$

$$\phi_K(x) = 1 - 2 \left(\frac{n-1}{n+1} \right)^n \exp \left[-2 \left(1 - \frac{1}{n^2} \right) x \right], \quad \text{when } x \rightarrow +\infty. \quad (2-21)$$

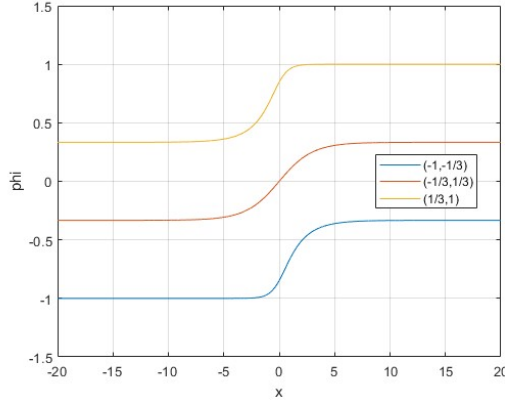


Figure 3: Kinks (no antikinks) when $n = 3$ in the ϕ^8 theory

(ii) **symmetric kink** $(-1/n, 1/n)$

$$\phi_K(x) = -\frac{1}{n} + \frac{2}{n} \left(\frac{n-1}{n+1} \right)^{1/n} \exp \left[\frac{2}{n} \left(1 - \frac{1}{n^2} \right) x \right], \quad \text{when } x \rightarrow -\infty. \quad (2-22)$$

$$\phi_K(x) = \frac{1}{n} - 2 \left(\frac{n-1}{n+1} \right)^n \exp \left[-\frac{2}{n} \left(1 - \frac{1}{n^2} \right) x \right], \quad \text{when } x \rightarrow +\infty. \quad (2-23)$$

Based on Equations above, the asymptotic form can be used to derive the boundary conditions for a general n .

3 The kink-antikink collision in the ϕ^8 Theory

In the last section they are all static kink solutions. A Lorentz transformation applied to the static solution yields a relativistic dynamics for the kink-antikink collisions [16]. Here, we consider a pair of kink-antikink moving towards each other with the same velocity v_{in} . Initially, the kink and antikink are separated by a distance of $2a$, and the general form of the field can be expressed as

$$\phi_{K\bar{K}}(x, t) = \phi_K [\gamma(x - v_{in}t + a)] + \phi_{\bar{K}} [\gamma(x + v_{in}t - a)] + p, \quad (3-1)$$

where γ is Lorentz factor, which can be expressed as

$$\gamma = \frac{1}{\sqrt{1 - v^2}}. \quad (3-2)$$

Here, v denotes the kink velocity normalized by the speed of light $c = 1$, and a represents the initial position of the kink. The p in Equation 3-1 is a constant which makes the configuration of kink-antikink satisfy the boundary condition. There are three different p for the corresponding sectors: (i) When $(-p_2, -p_1) = (-1, -1/n)$, $p = p_1$; (ii) When $(-p_1, p_1) = (-1/n, 1/n)$, $p = -p_1$; (iii) When $(p_1, p_2) = (1/n, 1)$, $p = -p_2$. In the previous research on ϕ^8 theory, due to the strong nonlinearity of the potential field as well as

the complexity and global internal modes, it is extremely challenging to apply the covariant coordinate method and make effective approximations. In ϕ^8 theory, for a potential parameter $n = p_2/p_1$, there exist six solitons with distinct configurations. The collision phenomena of soliton pairs vary with their different configurations and quantities [12]. This paper will focus on the kink dynamics for Topological sectors $n = 2$ and $n = 3$. We also present several cases where n takes other values.

3.1 Setup for $\phi_{K\bar{K}}$

Based on Equation 3-1, the relativistic formulation of the $\phi_{K\bar{K}}$ for a kink-antikink system moving with an initial velocity v_{in} and an initial separation $2a$ is considered, where the Lorentz factor γ is treated as an independent parameter. It takes on different expressions for different values of n .

(1) $n = p_2/p_1 = 2$

Based on the single soliton in Equation 2-11, we can get that $m = 0$ and $m = 5$ correspond to the kink and antikink, respectively. Together with its topological distribution sector $(1/2, 1)$, its relativistically covariant form can be written as

$$\phi_{0,5}(x) = \phi_0(\gamma(x - v_{in}t + a)) + \phi_5(\gamma(x + v_{in}t - a)) - 1. \quad (3-3)$$

Correspondingly, for the kink-antikink pair with $m = 1$ and $m = 4$ over sector $(-1/2, 1/2)$, and the other kink-antikink pair with $m = 2$ and $m = 3$ over sector $(-1, -1/2)$, the relativistically covariant forms of ϕ can be written as

$$\phi_{1,4}(x) = \phi_1(\gamma(x - v_{in}t + a)) + \phi_4(\gamma(x + v_{in}t - a)) - \frac{1}{2}, \quad (3-4)$$

$$\phi_{2,3}(x) = \phi_2(\gamma(x - v_{in}t + a)) + \phi_3(\gamma(x + v_{in}t - a)) + \frac{1}{2}, \quad (3-5)$$

here $\phi_m(x)$ is in Equation 2-11.

(2) $n = p_2/p_1 = 3$

For the case of $n = 3$, the potential field expression of a single soliton is rather complex by itself. Moreover, it also splits into two separate expressions in the potential field, and the corresponding kink-antikink expressions are complicated as well. For the sake of convenience in our discussion, we first describe the scenario where $v_{in} \cdot t < a$. When the kink is in the sector $(-1, -1/3)$, the $\phi_{K\bar{K}}$ is written as

(i) $x < -a + v_{in}t$,

$$\begin{aligned} \phi_{K\bar{K}}(x) = & -\frac{1}{3} \left\{ -\sqrt{1 - [\text{sech}(y_1)]^{\frac{2}{3}}} + \sqrt{2 + [\text{sech}(y_1)]^{\frac{2}{3}} - \frac{2 \tanh(y_2)}{\sqrt{1 - [\text{sech}(y_1)]^{\frac{2}{3}}}}} \right\} \\ & -\frac{1}{3} \left\{ \sqrt{1 - [\text{sech}(y_2)]^{\frac{2}{3}}} + \sqrt{2 + [\text{sech}(y_2)]^{\frac{2}{3}} + \frac{2 \tanh(y_2)}{\sqrt{1 - [\text{sech}(y_2)]^{\frac{2}{3}}}}} \right\} + \frac{1}{3}. \end{aligned} \quad (3-6)$$

(ii) $-a + v_{int} < x < a - v_{int}$

$$\begin{aligned} \phi_{K\bar{K}}(x) = & -\frac{1}{3} \left\{ -\sqrt{1 - [\operatorname{sech}(y_1)]^{\frac{2}{3}}} + \sqrt{2 + [\operatorname{sech}(y_1)]^{\frac{2}{3}} - \frac{2 \tanh(y_1)}{\sqrt{1 - [\operatorname{sech}(y_1)]^{\frac{2}{3}}}}} \right\} \\ & -\frac{1}{3} \left\{ -\sqrt{1 - [\operatorname{sech}(y_2)]^{\frac{2}{3}}} + \sqrt{2 + [\operatorname{sech}(y_2)]^{\frac{2}{3}} - \frac{2 \tanh(y_2)}{\sqrt{1 - [\operatorname{sech}(y_2)]^{\frac{2}{3}}}}} \right\} + \frac{1}{3}. \end{aligned} \quad (3-7)$$

(iii) $x > a - v_{int}$

$$\begin{aligned} \phi_{K\bar{K}}(x) = & -\frac{1}{3} \left\{ \sqrt{1 - [\operatorname{sech}(y_1)]^{\frac{2}{3}}} + \sqrt{2 + [\operatorname{sech}(y_1)]^{\frac{2}{3}} + \frac{2 \tanh(y_1)}{\sqrt{1 - [\operatorname{sech}(y_1)]^{\frac{2}{3}}}}} \right\} \\ & -\frac{1}{3} \left\{ -\sqrt{1 - [\operatorname{sech}(y_2)]^{\frac{2}{3}}} + \sqrt{2 + [\operatorname{sech}(y_2)]^{\frac{2}{3}} - \frac{2 \tanh(y_2)}{\sqrt{1 - [\operatorname{sech}(y_2)]^{\frac{2}{3}}}}} \right\} + \frac{1}{3}, \end{aligned} \quad (3-8)$$

When the potential field lies in the interval $(-1/3, 1/3)$, the $\phi_{K\bar{K}}$ is written as

(i) $x < -a + v_{int}$

$$\begin{aligned} \phi_{K\bar{K}}(x) = & -\frac{1}{3} \left\{ \sqrt{1 + [\operatorname{csch}(y_1)]^{\frac{2}{3}}} - \sqrt{2 - [\operatorname{csch}(y_1)]^{\frac{2}{3}} - \frac{2 \coth(y_1)}{\sqrt{1 + [\operatorname{csch}(y_1)]^{\frac{2}{3}}}}} \right\} \\ & -\frac{1}{3} \left\{ -\sqrt{1 + [\operatorname{csch}(y_2)]^{\frac{2}{3}}} + \sqrt{2 - [\operatorname{csch}(y_2)]^{\frac{2}{3}} + \frac{2 \coth(y_2)}{\sqrt{1 + [\operatorname{csch}(y_2)]^{\frac{2}{3}}}}} \right\} - \frac{1}{3}. \end{aligned} \quad (3-9)$$

(ii) $-a + v_{int} < x < a - v_{int}$

$$\begin{aligned} \phi_{K\bar{K}}(x) = & -\frac{1}{3} \left\{ \sqrt{1 + [\operatorname{csch}(y_1)]^{\frac{2}{3}}} - \sqrt{2 - [\operatorname{csch}(y_1)]^{\frac{2}{3}} - \frac{2 \coth(y_1)}{\sqrt{1 + [\operatorname{csch}(y_1)]^{\frac{2}{3}}}}} \right\} \\ & -\frac{1}{3} \left\{ \sqrt{1 + [\operatorname{csch}(y_2)]^{\frac{2}{3}}} - \sqrt{2 - [\operatorname{csch}(y_2)]^{\frac{2}{3}} - \frac{2 \coth(y_2)}{\sqrt{1 + [\operatorname{csch}(y_2)]^{\frac{2}{3}}}}} \right\} - \frac{1}{3}. \end{aligned} \quad (3-10)$$

(iii) $x > a - v_{int}$

$$\begin{aligned} \phi_{K\bar{K}}(x) = & -\frac{1}{3} \left\{ -\sqrt{1 + [\operatorname{csch}(y_1)]^{\frac{2}{3}}} + \sqrt{2 - [\operatorname{csch}(y_1)]^{\frac{2}{3}} + \frac{2 \coth(y_1)}{\sqrt{1 + [\operatorname{csch}(y_1)]^{\frac{2}{3}}}}} \right\} \\ & -\frac{1}{3} \left\{ \sqrt{1 + [\operatorname{csch}(y_2)]^{\frac{2}{3}}} - \sqrt{2 - [\operatorname{csch}(y_2)]^{\frac{2}{3}} - \frac{2 \coth(y_2)}{\sqrt{1 + [\operatorname{csch}(y_2)]^{\frac{2}{3}}}}} \right\} - \frac{1}{3}. \end{aligned} \quad (3-11)$$

When the potential field lies in the interval $(1/3, 1)$, the $\phi_{K\bar{K}}$ is written as

(i) $x < -a + v_{int}$

$$\begin{aligned} \phi_{K\bar{K}}(x) = & -\frac{1}{3} \left\{ -\sqrt{1 - [\operatorname{sech}(y_1)]^{\frac{2}{3}}} - \sqrt{2 + [\operatorname{sech}(y_1)]^{\frac{2}{3}} - \frac{2 \tanh(y_1)}{\sqrt{1 - [\operatorname{sech}(y_1)]^{\frac{2}{3}}}}} \right\} \\ & - \frac{1}{3} \left\{ \sqrt{1 - [\operatorname{sech}(y_2)]^{\frac{2}{3}}} - \sqrt{2 + [\operatorname{sech}(y_2)]^{\frac{2}{3}} + \frac{2 \tanh(y_2)}{\sqrt{1 - [\operatorname{sech}(y_2)]^{\frac{2}{3}}}}} \right\} - 1. \end{aligned} \quad (3-12)$$

(ii) $-a + v_{int} < x < a - v_{int}$

$$\begin{aligned} \phi_{K\bar{K}}(x) = & -\frac{1}{3} \left\{ -\sqrt{1 - [\operatorname{sech}(y_1)]^{\frac{2}{3}}} - \sqrt{2 + [\operatorname{sech}(y_1)]^{\frac{2}{3}} - \frac{2 \tanh(y_1)}{\sqrt{1 - [\operatorname{sech}(y_1)]^{\frac{2}{3}}}}} \right\} \\ & - \frac{1}{3} \left\{ -\sqrt{1 - [\operatorname{sech}(y_2)]^{\frac{2}{3}}} - \sqrt{2 + [\operatorname{sech}(y_2)]^{\frac{2}{3}} - \frac{2 \tanh(y_2)}{\sqrt{1 - [\operatorname{sech}(y_2)]^{\frac{2}{3}}}}} \right\} - 1. \end{aligned} \quad (3-13)$$

(iii) $x > a - v_{int}$

$$\begin{aligned} \phi_{K\bar{K}}(x) = & -\frac{1}{3} \left\{ \sqrt{1 - [\operatorname{sech}(y_1)]^{\frac{2}{3}}} - \sqrt{2 + [\operatorname{sech}(y_1)]^{\frac{2}{3}} + \frac{2 \tanh(y_1)}{\sqrt{1 - [\operatorname{sech}(y_1)]^{\frac{2}{3}}}}} \right\} \\ & - \frac{1}{3} \left\{ -\sqrt{1 - [\operatorname{sech}(y_2)]^{\frac{2}{3}}} - \sqrt{2 + [\operatorname{sech}(y_2)]^{\frac{2}{3}} - \frac{2 \tanh(y_2)}{\sqrt{1 - [\operatorname{sech}(y_2)]^{\frac{2}{3}}}}} \right\} - 1. \end{aligned} \quad (3-14)$$

Here $y_1 = \frac{8}{9}\gamma(x - a + v_{int})$, $y_2 = \frac{8}{9}\gamma(-x - a + v_{int})$.

(3) Other n

For a general value of n , an explicit expression for the potential field is not straightly available except for the cases of $n = 2$ and $n = 3$. The general solution can only be derived by combining mathematical or numerical approximations of the boundary conditions with numerical methods by now. This content will be presented on in the Section 3.2 and will not be discussed in excessive detail here.

3.2 Set up of the boundary conditions

In the numerical calculation, the boundary conditions are different for the explicit and implicit cases. We present them in the following.

(1) Explicit cases

To do numerical simulations, we present the initial boundary conditions. If an explicit analytical solution or an explicit approximate expression of kink is available, the initial

boundary condition can be directly presented via the finite difference method. In general, the boundary conditions required for numerical simulations can be obtained by combining the derived $\phi_{K\bar{K}}(x, t)$ with the first-order finite difference method, whose general expression is given by

$$\frac{\partial\phi_{K\bar{K}}}{\partial x}\Big|_{\Delta x, \Delta t \rightarrow 0, t=0} \approx \frac{\phi_{K\bar{K}}(x + \Delta x, 0) - \phi_{K\bar{K}}(x, 0)}{\Delta x}. \quad (3-15)$$

According to Equation 3-1, Equation 3-15 can be rewritten as

$$\begin{aligned} \frac{\partial\phi_{K\bar{K}}}{\partial x}\Big|_{\Delta x, \Delta t \rightarrow 0, t=0} \approx & \frac{1}{\Delta x} \{ \phi_K[\gamma(x - v_{in}\Delta t + a)] + \phi_{\bar{K}}[\gamma(x + v_{in}\Delta t - a)] \\ & - \phi_K[\gamma(x + a)] - \phi_{\bar{K}}[\gamma(x - a)] \}. \end{aligned} \quad (3-16)$$

(2) Implicit cases

In the interval $0 < p_1 < |\phi| < p_2$, x can be expressed as an explicit function of ϕ , denoted as $x = f(\phi_K)$. For a kink, the corresponding ϕ_K can be solved by the nonlinear equation $f(\phi_K) - x = 0$ over the interval $[-x_{max}, x_{max}]$ (x_{max} is the boundary), which gives the Dirichlet boundary condition. Based on Equation 3-16, the Neumann boundary condition can be derived by solving the Equation $f(\phi_K) - (x + v_{in}k) = 0$ (here k denotes the time bin Δt) in combination with the Dirichlet boundary condition. For a soliton pair with the kink initially at $-a$ and the antikink at a , the general Dirichlet boundary condition for the kink is given by $x + a = f(\phi_K)$, and that for the antikink by $x - a = -f(\phi_{\bar{K}})$; the general Neumann boundary condition for the kink is $x + a - v_{in}k = f(\phi_K)$, and that for the antikink is $x - a + v_{in}k = -f(\phi_{\bar{K}})$. Based on the above analysis, the following formulas are obtained

$$\frac{1}{2(p_2^2 - p_1^2)} \ln \left[\left(\frac{\phi_K(x) - p_1}{\phi_K(x) + p_1} \right)^{1/p_1} \cdot \left(\frac{\phi_K(x) + p_2}{p_2 - \phi_K(x)} \right)^{1/p_2} \right] - (x + a) = 0, \quad (3-17)$$

$$-\frac{1}{2(p_2^2 - p_1^2)} \ln \left[\left(\frac{\phi_{\bar{K}}(x) - p_1}{\phi_{\bar{K}}(x) + p_1} \right)^{1/p_1} \cdot \left(\frac{\phi_{\bar{K}}(x) + p_2}{p_2 - \phi_{\bar{K}}(x)} \right)^{1/p_2} \right] - (x - a) = 0, \quad (3-18)$$

$$\frac{1}{2(p_2^2 - p_1^2)} \ln \left[\left(\frac{\phi_K(\bar{x}) - p_1}{\phi_K(\bar{x}) + p_1} \right)^{1/p_1} \cdot \left(\frac{\phi_K(\bar{x}) + p_2}{p_2 - \phi_K(\bar{x})} \right)^{1/p_2} \right] - (\bar{x} + a) = 0, \quad (3-19)$$

$$-\frac{1}{2(p_2^2 - p_1^2)} \ln \left[\left(\frac{\phi_{\bar{K}}(\bar{x}) - p_1}{\phi_{\bar{K}}(\bar{x}) + p_1} \right)^{1/p_1} \cdot \left(\frac{\phi_{\bar{K}}(\bar{x}) + p_2}{p_2 - \phi_{\bar{K}}(\bar{x})} \right)^{1/p_2} \right] - (\bar{x} - a) = 0. \quad (3-20)$$

Here $\bar{x} = x - v_{in}k$ in Equation 3-19 and $\bar{x} = x + v_{in}k$ in Equation 3-20. The Newton's method or the pseudospectral method [13] can be adopted for the numerical solution. In this work, we adopt the Newton's method. The Dirichlet and Neumann boundary conditions can be derived by combining with the first-order finite difference method

$$\phi_{K\bar{K}}\Big|_{\Delta x, \Delta t \rightarrow 0, t=0} = \phi_K(x) + \phi_{\bar{K}}(x) + p, \quad (3-21)$$

$$\frac{\partial\phi_{K\bar{K}}}{\partial x}\Big|_{\Delta x, \Delta t \rightarrow 0, t=0} = \frac{(\phi_K(\bar{x}) + \phi_{\bar{K}}(\bar{x})) - (\phi_K(x) + \phi_{\bar{K}}(x))}{k}. \quad (3-22)$$

4 Numerical results

4.1 The numerical illustration of collisions

In this paper, a numerical scheme combining the finite difference method introduced above with the Runge-Kutta method [17] is adopted to solve the time-dependent potential field. The finite difference method discretizes the spatial derivatives of the wave equation, thus yielding a set of coupled ordinary differential equations with time as the independent variable. Standard methods (e.g., the Runge-Kutta method) is used to solve these coupled ordinary differential equations. Based on the former analysis, the ϕ^8 theory can be sorted by different n values. Here we use the Dirichlet boundary condition, and set that the spatial boundary is far from the initial kink and antikink pair. We make some preliminary numerical tests, and find that $x_{max} = 200$ for $v < 0.7$ and $x_{max} = 300$ for $v > 0.7$ are proper. Thus, we consider $x \in [-200, 200]$ and $t \in [0, 300]$ for $t \in [0, 400]$ in the numerical simulations. With these settings, the boundary perturbations have almost no effect on the core region of interest. To ensure the computational feasibility, the step bins are set as $h = \Delta x = k = \Delta t = 0.05$.

To manifest the kink and anti-kink collisions, we consider three cases of n with different topological sectors. The initial velocity v is varied to find the special bounce states.

(1) $n = p_2/p_1 = 2$

Here we consider that $\phi_{K\bar{K}}$ is inclined to the vacuum boundary at $|x| = 200$, and the initial distance from the kink to the center is set as $a = 10$. As presented in Section 2.1, there are three fundamental topological sectors, $(-1, -1/2)$, $(-1/2, 1/2)$, and $(1/2, 1)$. The sector $(-1/2, 1/2)$ was named as inner sector, while the other two sectors were named as the outer sector [13]. We will study these sectors in the follows.

(i) Topological sector $(-1, -1/2)$

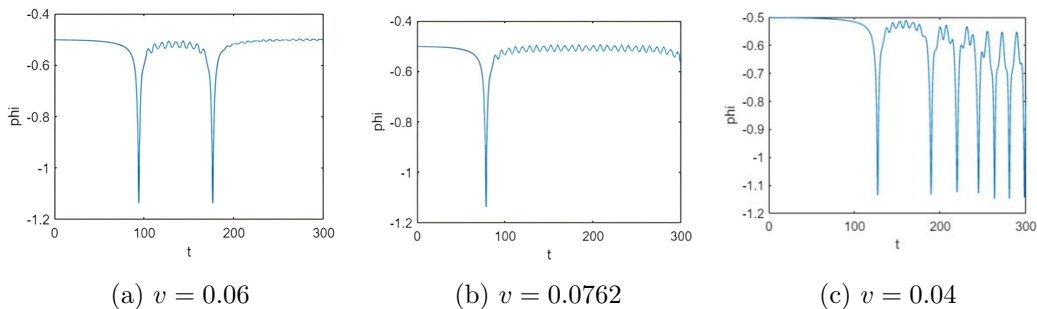


Figure 4: 2D plot of the $\phi_{K\bar{K}}$ at $x = 0$. From left to right panels, the initial velocities are $v = 0.06$, $v = 0.0762$ and $v = 0.04$, respectively.

Figure 4 illustrates the evolutions of $\phi_{K\bar{K}}$ at $x = 0$ for $t \in [0, 300]$. It can be seen that the number of bounces are 2, 1 and 7 at the left, middle and right panels, respectively. The corresponding 3D plots are presented in Figure 5. For $v = 0.04$, the soliton pair

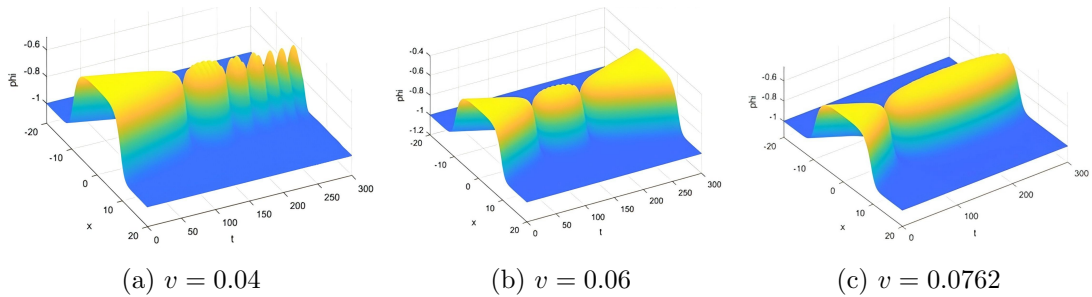


Figure 5: 3D plot of $\phi_{K\bar{K}}$ with the initial velocities $v = 0.04$, $v = 0.06$, and $v = 0.0762$, respectively.

forms a long-lived bound oscillatory state, known as the bion. In this case, the initial kinetic energy is partly converted to both the vibration energy, and the remaining kinetic energy is insufficient to overcome the long-range attractive potential after each collision. For $v = 0.06$, the kink-antikink pair initially separates after the first collision, turning to a transient vibrational state. They subsequently re-approach, collide for a second time, and then escape to infinity. This is a case of escaping state. In such process, the kinetic energy is converted to the internal vibrational modes after first collisions. After the second collision, the vibrational energy is returned back to the kinetic energy, which is sufficient to overcome the long-range mutual attraction. For $v = 0.0762$, the soliton pair separates after the initial collision, but exhibits a turning back tendency for a long-term time duration $\Delta t \sim 200$. Such long-term oscillation is common in our ϕ^8 simulations, and can be considered as a characteristic of ϕ^8 theory. After first collision, the soliton pair reposit some energy in the vibrational mode, and the remaining kinetic energy could not overcome the long-range attraction, leading to a next collision in the extended time intervals. These results demonstrate that the final states of kink-antikink pairs is not a simple function of initial velocity, but is governed by the non-linear partition of initial energy into the vibrations, long-range interactions, and kinetic energy.

(ii) *Topological sector* $(-1/2, 1/2)$

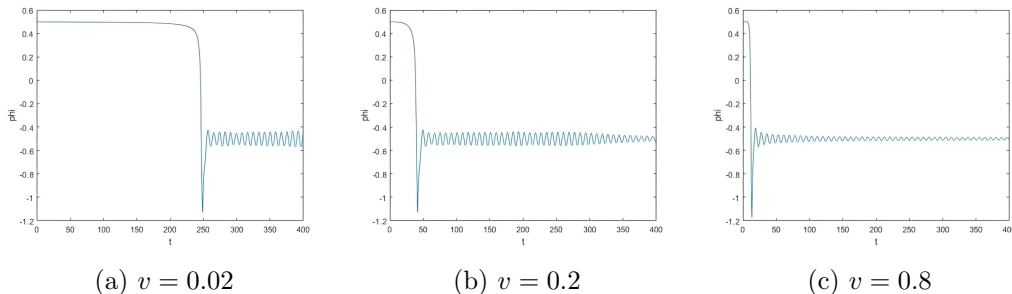


Figure 6: 2D plot of the $\phi_{K\bar{K}}$ at $x = 0$. From left to right panels, the velocities are $v = 0.02$, $v = 0.2$ and $v = 0.8$, respectively.

Figure 6 depicts the time evolution of $\phi_{K\bar{K}}$ at $x = 0$ for the sector $(-1/2, 1/2)$. We present three cases with $v = 0.02, 0.2$, and 0.8 , respectively. The corresponding 3D plots are presented in Figure 7. In all three cases shown, the kink-antikink pair undergoes direct

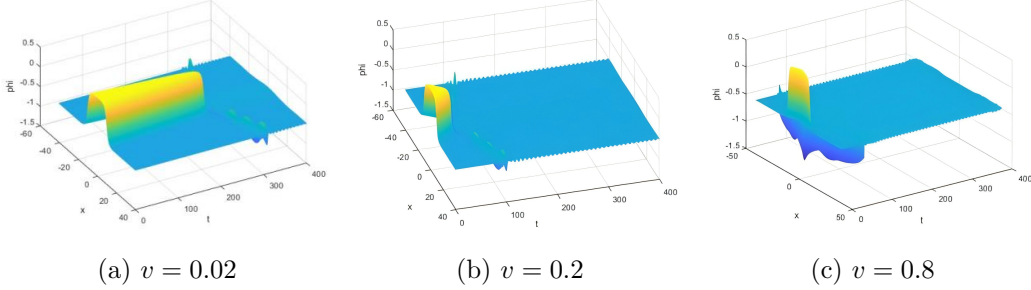


Figure 7: 3D plot of $\phi_{K\bar{K}}$ with the initial velocities $v = 0.02$, $v = 0.2$ and $v = 0.8$, respectively.

annihilation after the initial collision, with the field relaxing to the vacuum at the spatial boundary. No escaping or bound state is observed. Some radiation escape to the boundary with a out-going velocity exceeding the incident velocity. This annihilation behavior is found to be the unique outcome for the full range of initial velocities within this topological sector. D. Bazeia et al. has reported the annihilation for ϕ^8 theory for the inner sector $(-0.82, 0.82)$ at $v = 0.2$ [13]. However, the author did not study the full velocity range. From the view of energy, all the initial kinetic energy and configuration energy are turned into the radiation and vibration mode of the vacuum. To understand this phenomenon, we also presented its energy density plot. In Figure 8, the originally concentrated energy

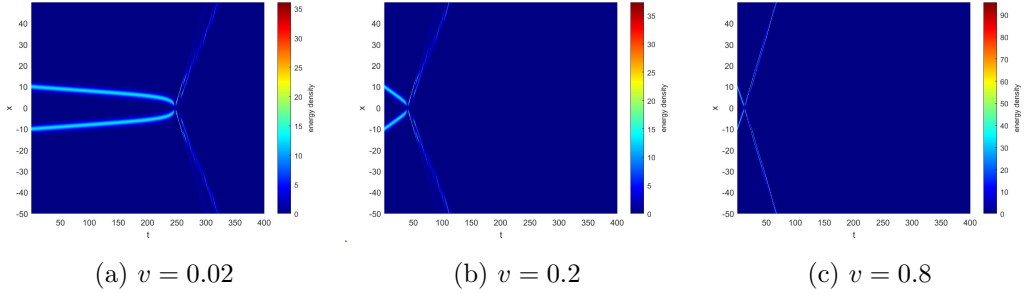


Figure 8: energy density plots of $\phi_{K\bar{K}}$ with the initial velocities $v = 0.02$, $v = 0.2$ and $v = 0.8$, respectively.

density can no longer maintain the localized soliton configuration and collapses abruptly. The localized energy is fully radiated toward both boundary sides in the form of dispersive wave modes.

(iii) *Topological sector* $(1/2, 1)$

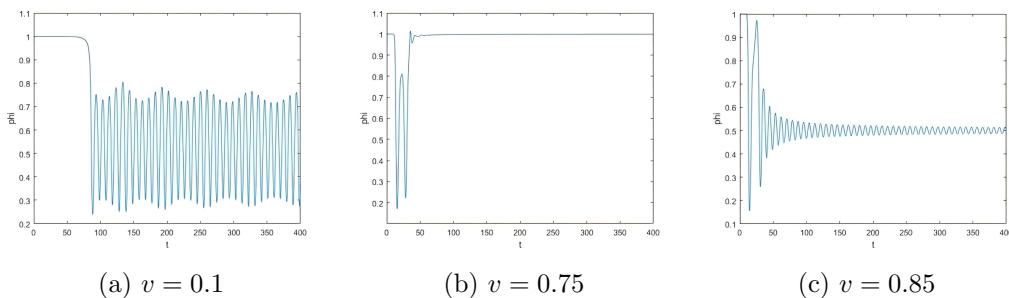


Figure 9: 2D plot of the $\phi_{K\bar{K}}$ at $x = 0$. From left to right panels, incident velocities are $v = 0.1$, $v = 0.75$ and $v = 0.85$, respectively.

Figure 9 demonstrates the time evolution of $\phi_{K\bar{K}}$ at $x = 0$ for the topological sector $(1/2, 1)$. In the left panel, the kink-antikink soliton pair oscillates near the vacuum after collision over the range $t \in [0, 400]$. In the middle panel, the number of bounces is two, and the pair reflects back. In the right panel, different from the panel (a), the kink-antikink soliton pair first bounces one time, and then quickly annihilates to vacuum in a manner similar to the phenomenon in topological sector $(-1/2, 1/2)$. The 3D plots in conjunction with the velocities in Figure 9 is presented below.

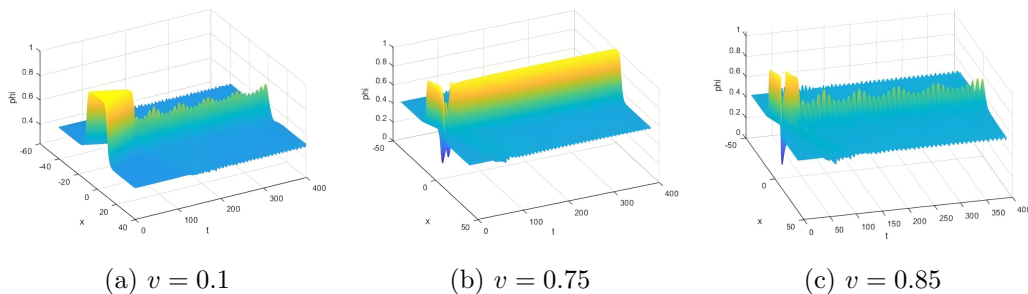


Figure 10: 3D plot of $\phi_{K\bar{K}}$ with the incident velocities $v = 0.1$, $v = 0.75$ and $v = 0.85$, respectively.

Figure 9 and Figure 10 illustrate the time evolution of $\phi_{K\bar{K}}$ over the range of $x \in [-200, 200]$, revealing three distinct dynamical outcomes. These outcomes can be interpreted by analyzing the balance between the initial kinetic energy and the system's long-range potential. When the kinetic energy of solitons is too low to overcome the strong short-range attractive force after the collision, the system directly turns into a bound state. When the initial kinetic energy is slightly below but very close to the critical escaping energy, the pair is temporarily confined by the short-range attraction, resulting in a second bounce. The residual kinetic energy is ultimately sufficient to overcome the long-range confinement. There may be more than one vibration frequency in such case. After the first bounce, ϕ cannot return to 1 with some energy radiation. The energy distributes among the vibration, the radiation and the kinetic components. There are some energy

transition among them. For the case of $v = 0.85$, the energy transfer process is complex, which is uncommon in the kink and anti-kink collisions. After the first bounce, the system undergoes substantial energy dissipation, which rapidly depletes the pair's kinetic energy. The bion decays to the vacuum state, with some radiation escaping to the boundary.

(2) $n = p_2/p_1 = 3$

(i) *Topological sector* $(-1, -1/3)$

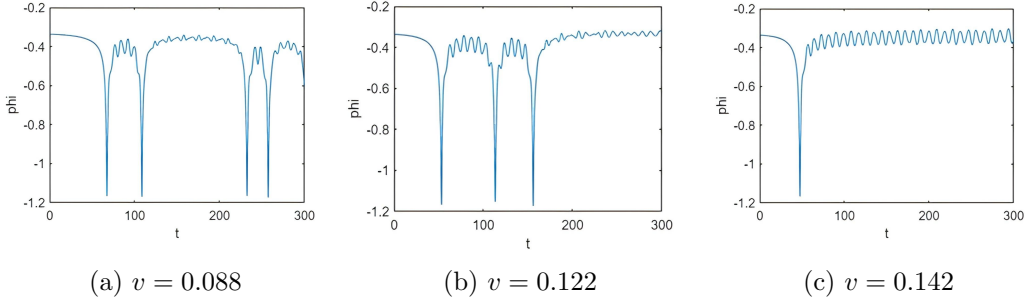


Figure 11: 2D plot of the $\phi_{K\bar{K}}$ at $x = 0$. From left to right panels, incident velocities are $v = 0.088$, $v = 0.122$ and $v = 0.142$, respectively.

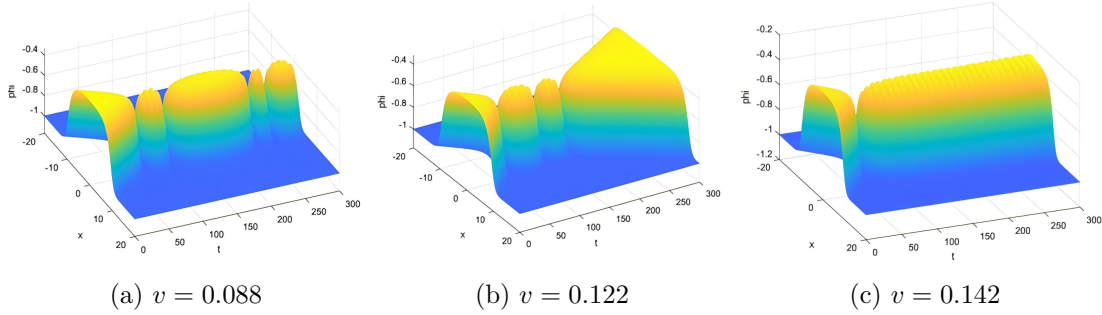


Figure 12: 3D plot of $\phi_{K\bar{K}}$ with the initial velocities $v = 0.088$, $v = 0.122$ and $v = 0.142$, respectively.

Figure 11 and Figure 12 demonstrate the time evolution of $\phi_{K\bar{K}}$ for the topological sector $(-1, -1/3)$. For $v = 0.088$, the kink and antikink pair undergoes four bounces before $t = 300$. For $v = 0.122$, the soliton pair escapes after three bounces. For a higher velocity of $v = 0.142$, the pair escapes immediately after the first collision. These three cases reveal a transition from multi-bounce resonances to direct escape as the initial velocity v increasing. Ignoring the incident velocities, these collision phenomena are similar to the collisions in topological sector $(-1, -1/2)$ of $n = 2$, and the energy transfer processes are also similar which will not be repeated here.

(ii) Topological sector $(-1/3, 1/3)$

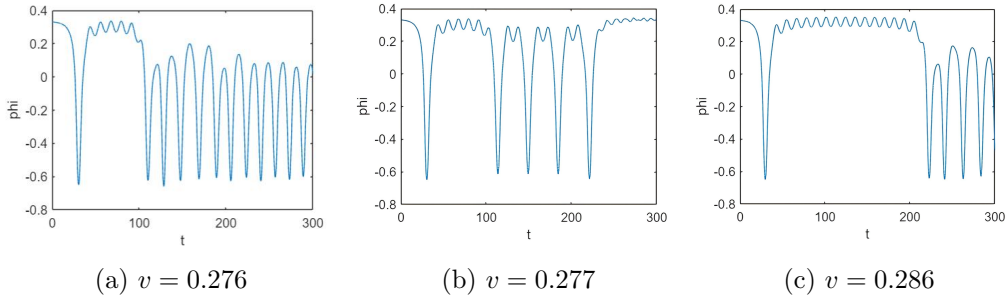


Figure 13: 2D plot of the $\phi_{K\bar{K}}$ at $x = 0$. Incident velocities are $v = 0.276$, $v = 0.277$ and $v = 0.286$, respectively.

The evolution of the kink-antikink field configuration, $\phi_{K\bar{K}}(x, t)$, was simulated over the domain $x \in [-200, 200]$ and $t \in [0, 300]$. The resulting dynamics reveal a rich variety of escape scenarios dependent on the initial collision velocity v . Figure 13 manifests the collision phenomena for the sector $(-1/3, 1/3)$. In the left panel, the soliton pair shows a bounce first, and then forms the bion state after the second collision. In the middle panel, the pair escapes successfully after 5 bounces. In the right panel, the soliton pair separates for a long time after the first collision, with the time duration being about 200, and forms a bion state upon the second collision. 3D plots are presented below in conjunction with incident velocities in Figure 14.

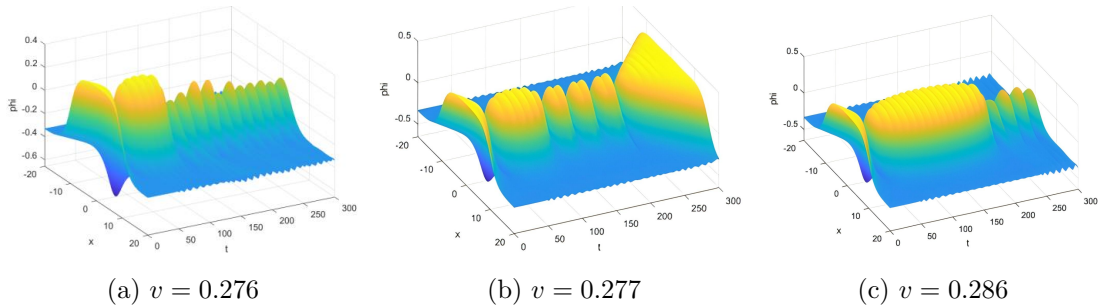


Figure 14: 3D plot of $\phi_{K\bar{K}}$ with the initial velocities $v = 0.276$, $v = 0.277$ and $v = 0.286$, respectively.

For $v = 0.276$, the kink-antikink pair separates for a while and then form a bion state. The time intervals between successive collisions exhibit a non-uniform pattern, approximately following a long-short sequence before the final escape. This sequence can be understood through an energy exchange mechanism. Initially, the pair possesses sufficient kinetic energy to overcome the short-range attractive potential, resulting in a long separation. Following the first collision, energy is transferred to the internal mode excitation, leading to less energy to escape or separate for a while. After the second collision, the internal modes disappear and the pair form a bion state. Simultaneously, ϕ cannot return

to $1/3$ and forms a lower bion state. The saw-toothed boundary indicates that some energy dissipates into boundary.

For $v = 0.277$, a more complex five-bounce escape scenario is observed. Following an initial collision, the pair undergoes an extended separation of approximately 80 time units. Subsequently, they experience three more bounces with relatively uniform time intervals before finally escaping. The vibration modes exist at all bounce processes, but with different frequencies and amplifications.

For $v = 0.286$, the pair initially separates over an extended period of approximately 200 time units. However, unlike the previous cases, this separation does not culminate in escape. Instead, the pair re-approaches and forms a lower bion state.

Notably, the five-bounce escape scenario observed at $v = 0.277$ represents, up to our knowledge, the first reported instance of such high-order bouncing in the ϕ^8 kink-antikink model. This result provides pivotal numerical evidence for high-order bounce resonance in this system and supports the theoretical conjecture proposed by [7, 18], which stated that the number of bounces during soliton escape could exceed four. The phenomenon of high-order bounces in kink-antikink collisions reveals the energy exchange between translational motion, internal vibrational modes and potential energy of kinks. Such multiple bounces also show the existence of long-lived internal excitations, which allows the kink and antikink to repeatedly approach, collide, and separate before finally escaping.

(iii) *Topological sector* $(1/3, 1)$

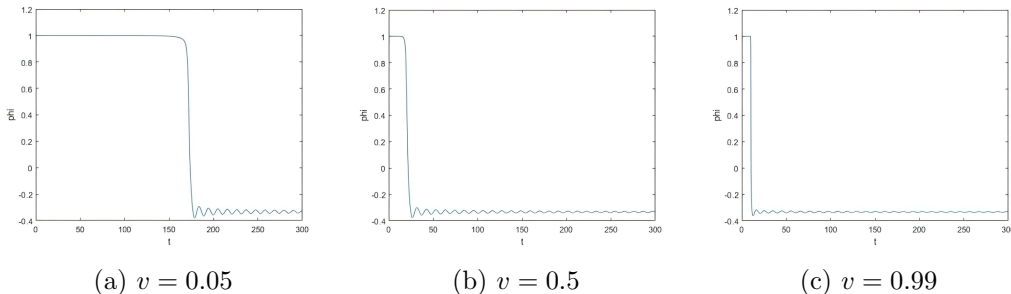


Figure 15: 2D plot of the $\phi_{K\bar{K}}$ at $x = 0$. Incident velocities are $v = 0.136$, $v = 0.277$ and $v = 0.286$, respectively.

Figure 15 demonstrates the time evolution of $\phi_{K\bar{K}}$ at $x = 0$ for the sector $(1/3, 1)$. The corresponding 3D plots are presented in Figure 16. Figure 15 show that in all three cases, the kink-antikink pair neither reflects back nor forms a bion state after the first collision. Instead, it forms a new soliton pair and changes the topological sector to $(-1/3, 1/3)$. Then, the soliton pair escape to infinity, and the vibration at vacuum $1/3$ remains at all spatial grids. This behavior is unique for the full range of initial velocities within this topological sector. To understand this phenomenon, we also presented its energy density plot in Figure 17. Such topological sector changing is known in the sine-Gordon model [19, 20, 21], as well as in ϕ^8 model [13].

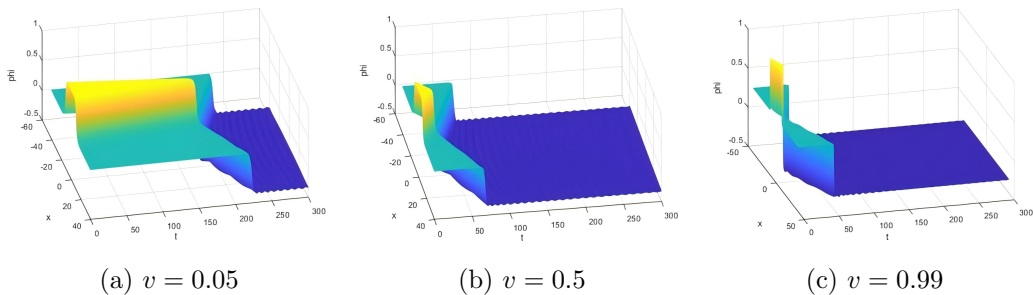


Figure 16: 3D plot of $\phi_{K\bar{K}}$ with the initial velocities $v = 0.05$, $v = 0.5$ and $v = 0.99$, respectively.

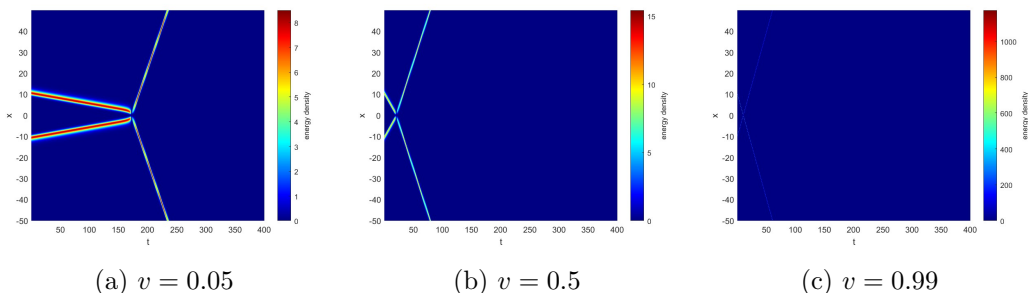


Figure 17: energy density plots of $\phi_{K\bar{K}}$ with the initial velocities $v = 0.05$, $v = 0.5$ and $v = 0.99$, respectively.

(3) Other n values

The boundary conditions employed herein are derived in section 3.2 by using the mathematical approximations. The numerical calculation considers methods such as the Newton-Raphson and pseudospectral methods. By combining these initial configurations with the fourth-order Runge-Kutta (RK4) method, the time evolution of the field with other n values can be obtained. One specific case with topological sector $(0.38005, 1)$ at $v = 0.1$ is presented in Figure 18.

It was observed that the kink-antikink pair first changes the sector after the first collision, from the outer sector $(0.38005, 1)$ to the inner sector $(-0.38005, 0.38005)$. Then, the system subsequently returns back to the outer sector $(0.38005, 1)$, and forms a bion state. This process, up to our knowledge, is also observed for the first time for ϕ^8 theory. The topological charge of the inner sector $(-0.38005, 0.38005)$ is larger than that of the outer sector $(0.38005, 1)$, which ensures that the system returns to the bion state with fundamental topological charges.

In Figure 19, a kink-antikink pair in the outer sector $(0.7, 1)$ with $v = 0.698$ can form a bion state immediately after collision, and subsequently achieve successful escape. The post-collision bion state bounces six times. It is interesting to notice that the second bounce is a 'dwarf' one, as well as the bounces after the six one. The field at $x = 0$ did not returns back to the vacuum 1, and its duration time is smaller than other bounces. We

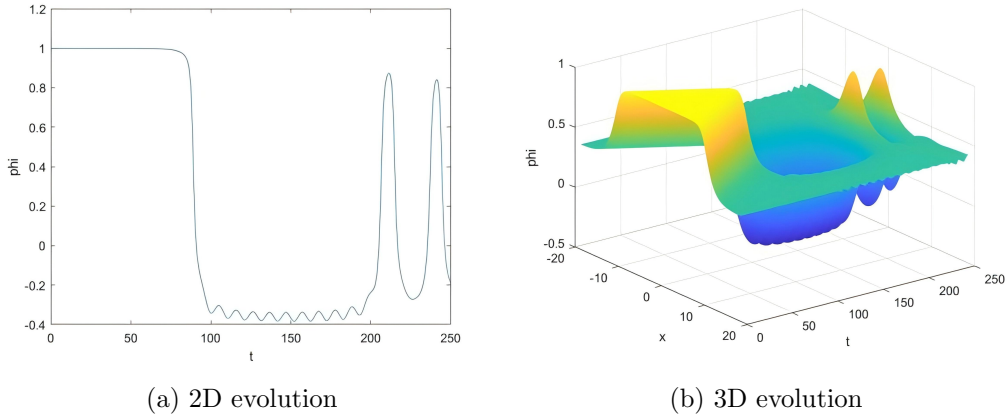


Figure 18: 2D and 3D plots of kink-antikink collision in the topological sector $(0.38005, 1)$ at $v = 0.1$

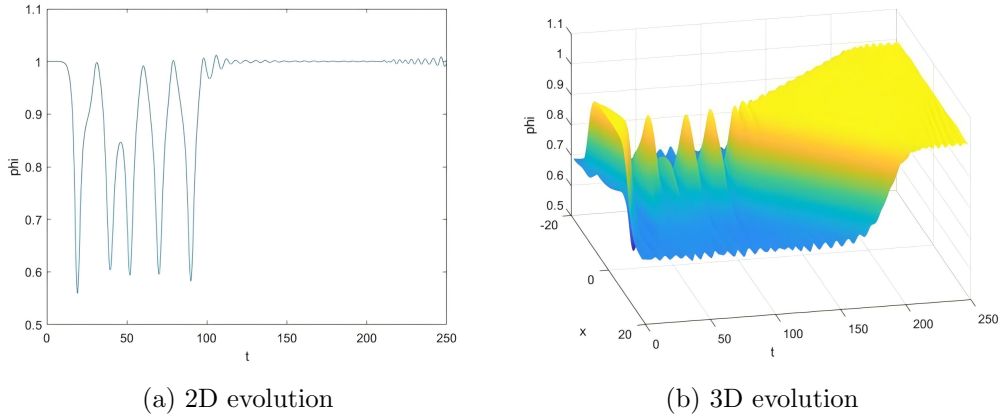


Figure 19: 2D and 3D plots of kink-antikink in the Topological sector $(0.7, 1)$ at $v = 0.698$

also notice that the duration of the first bounce is slightly larger than that of bounces from the third to the sixth. At the boundary, the saw pattern indicates that some radiation leaks away. There may be more than one vibration frequency in such case. The second bounce and bounces after the seventh have shorter duration time than the first and third to sixth bounces. The energy distributes among the vibration, the radiation and the kinetic components, and some energy transits among them.

A closely related dynamical process is observed at a slightly higher initial velocity $v = 0.69797$ in Figure 20. Here, the kink-antikink pair first forms a relatively high and uniform bion state after collision. Over time, this high-energy bion dissipates energy through radiation, transitioning to the 'dwarf' bion state with shorter resonance time and lower amplitude. The final states exhibits a wave packet with a profile resembling a beat frequency phenomenon.

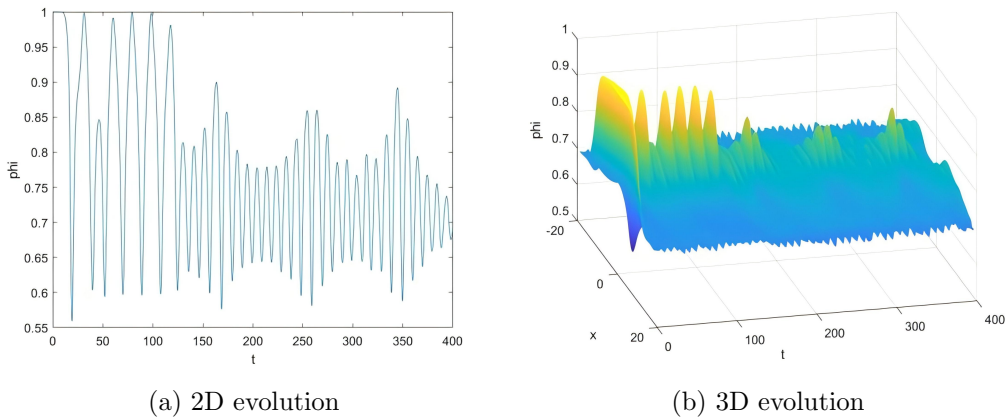


Figure 20: 2D and 3D plots of kink-antikink in the Topological sector $(0.7, 1)$ at $v = 0.69797$

4.2 The rich collision phenomena for different topological sector

To show the collision phenomena in the whole range of v_{in} , we plot the $v_{in} - v_{out}$ and $v_{in} - t$ (t is the outgoing time) for different topological sectors. The step size of v_{in} is taken as 0.001. In numerical calculation, v_{out} measures the velocity of solitons from the last bounce to the boundary. The number of bounce is counted when $\phi(x = 0)$ exceeds the range of topological sector. The setup of the numerical calculation is referred to Section 4.1. Here potential $U = dV/d\phi$. Following [8], we could also obtain the Schrödinger like equation

$$-\eta'' + U(x)\eta = \omega^2\eta. \quad (4.1)$$

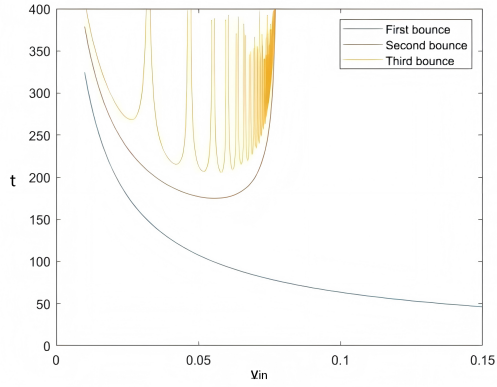
The numerical solution for this equation are also considered.

(1) $n = p_2/p_1 = 2$

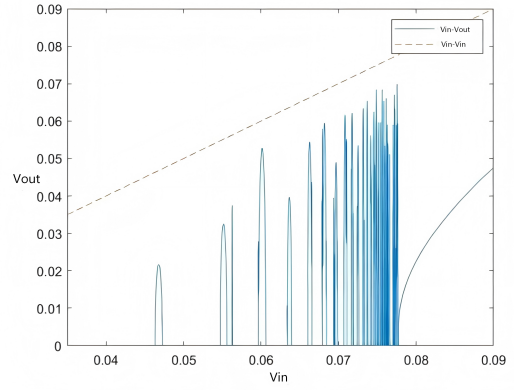
(i) *Topological sector $(-1, -1/2)$*

Figure 21 reveals that, within this topological sector, the collision exhibits intricate escape windows up to the critical velocity $v_c \approx 0.0777$. Beyond the critical velocity, the soliton pair escapes. In Figure 22, the left panel shows the $v_{in} - v_{out}$ plot for the two and three bounces, and the right panel shows that for the three and four bounces. The v_{in} in the right panel is a zoomed regime in the left panel. This shows the self-similar fractal structure for the soliton collisions, known in ϕ^4 and ϕ^6 theories [19, 20].

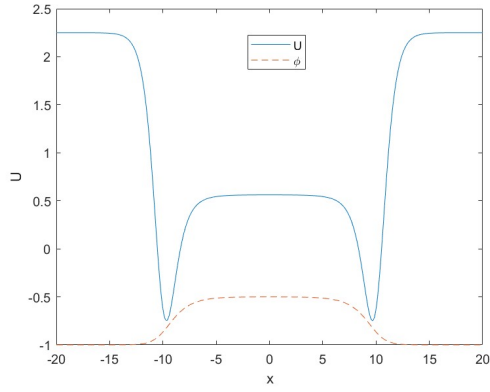
The rich collision behaviors are very similar to the collision phenomena in ϕ^6 theory [8]. It was indicated that, even though there are no shape modes in kinks of ϕ^6 theory, the ordered antikink and kink configuration could form a central potential well, which induces de-localized mode responsible for the rich collision phenomena [21, 22, 23]. We also plot the potential U for both the $K\bar{K}$ pair and the $\bar{K}K$ pair in Figure 21c and Figure 21d, respectively. It reveals that $K\bar{K}$ pair has a central well and $\bar{K}K$ pair has a raised central plateau. The frequency ω^2 as a function of half distance of soliton pair a is also plotted



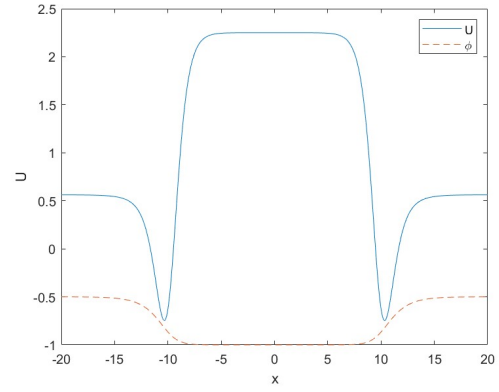
(a) $v_{in} - t$



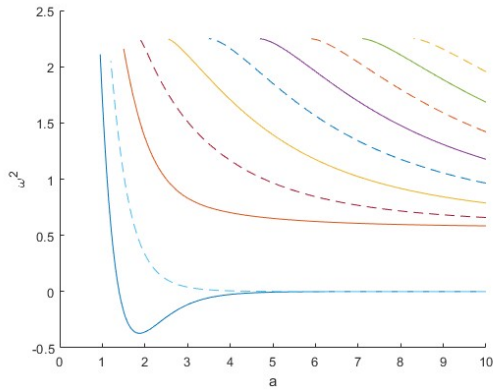
(b) $v_{in} - v_{out}$



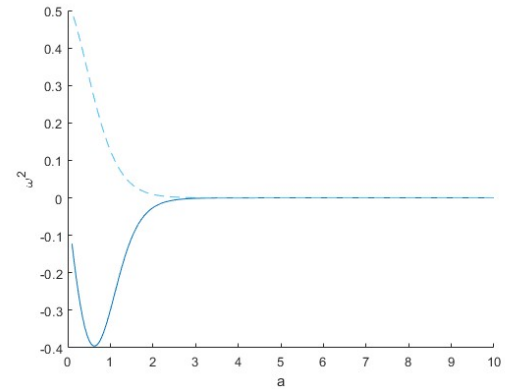
(c) $K\bar{K}$ pair potential $U(x)$



(d) $\bar{K}K$ pair potential $U(x)$

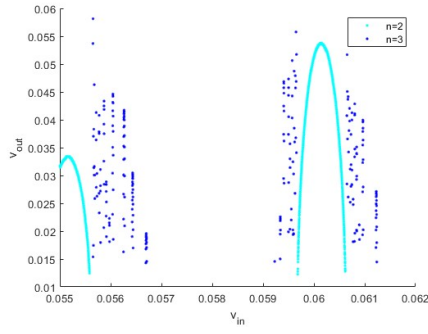


(e) $K\bar{K}$ pair spectrum

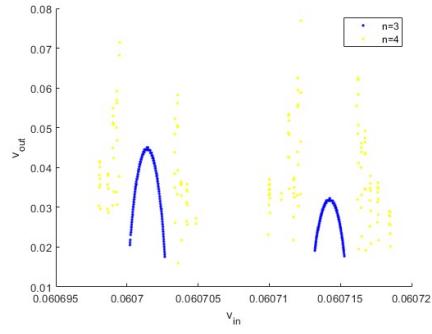


(f) $\bar{K}K$ pair spectrum

Figure 21: Topological sector $(-1, -1/2)$. In panel (e), the solid and dash lines represent the even and odd bound states for $K\bar{K}$ pair.



(a) $v_{in} \in [0.055, 0.062]$

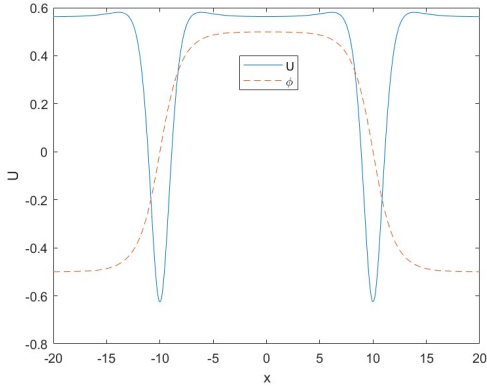


(b) $v_{in} \in [0.060695, 0.060702]$

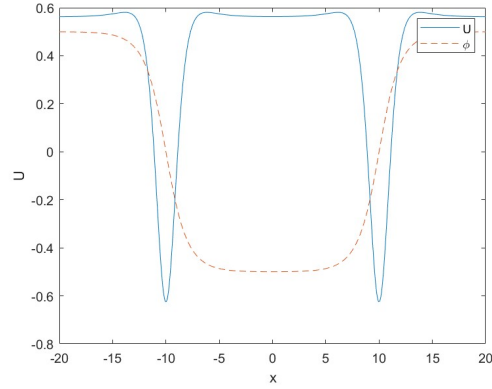
Figure 22: Fractal structure for topological sector $(-1, -1/2)$

in panel (e) and (f). From which, we could also observe that the $K\bar{K}$ pair has rich bound states, and the $\bar{K}K$ pair has no bound states.

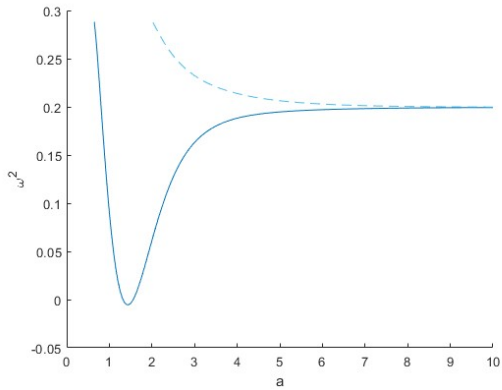
(ii) *Topological sector $(-1/2, 1/2)$*



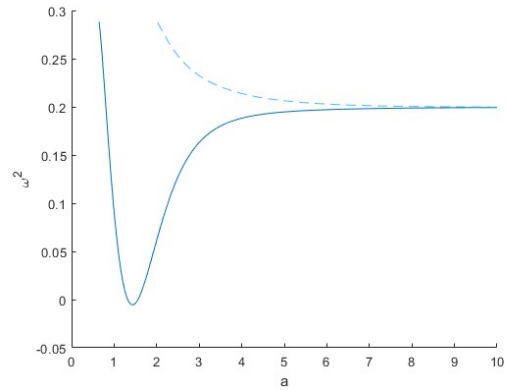
(a) $K\bar{K}$ potential $U(x)$



(b) $\bar{K}K$ potential $U(x)$



(c) $K\bar{K}$ pair spectrum



(d) $\bar{K}K$ pair spectrum

Figure 24: Topological sector $(-1/2, 1/2)$

There is no escape window in this topological sector, which has been indicated in Figure 7 and Figure 9 in Section 4.1. Within this sector, the kink-antikink pair undergoes annihilation after the initial collision with any given incident velocity. Thus, there is no fractal structure. Figure 24 reveals that the potential $U(x)$ of $K\bar{K}$ and $\bar{K}K$ pairs shows separated double-well, and the central plateau between wells is slightly concave. The annihilation behavior may be induced by this symmetrical potential. The spectrum shows no bound state.

(iii) *Topological sector* $(1/2, 1)$

For this topological sector, Figure 25 reveals a distinct structure. Unlike the dense cluster of escape windows in the sector $(-1, -1/2)$, the escape window does not appear until the velocity $v_{in} \approx 0.87$. In contrast with ϕ^6 in [8], the pair is trapped only one time before the critical velocity. There is no fractal structure in this topological sector. Figure 25c reveals that $K\bar{K}$ pair has a raised central plateau. We also plot the potential U for the $\bar{K}K$ pair in Figure 25d, which shows a central well. The collision phenomena for the $\bar{K}K$ in the sector $(1/2, 1)$ are the same for the $K\bar{K}$ in the sector $(-1, -1/2)$, which may due to that the potential $U(x)$ for these two cases are the same. The spectrum of $K\bar{K}$ shows no bound state, while the spectrum of $\bar{K}K$ shows rich bound states.

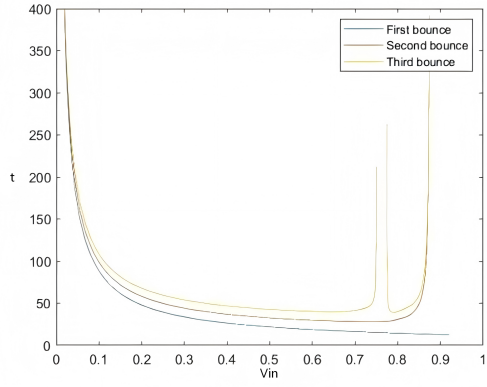
(2) $n = p_2/p_1 = 3$

(i) *Topological sector* $(-1, -1/3)$

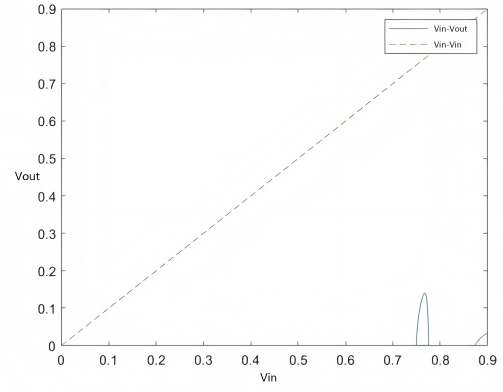
From Figure 26b, we obtain that the critical velocity is $v_c \approx 0.14$. The dynamical results for this case is similar to that in Figure 21, and is not repeated here for brevity. Figure 26c reveals that $K\bar{K}$ pair has a central well. We also plot the potential $U(x)$ for the $\bar{K}K$ pair in Figure 26d, which shows a raised central plateau. Here, the potential of the $\bar{K}K$ pair is similar to that of the $K\bar{K}$ pair in sector $(1/3, 1)$, see Figure 30. The $v_{in} - v_{out}$ plot of $K\bar{K}$ pair shows the fractal structure, as indicated in Figure 27.

(ii) *Topological sector* $(-1/3, 1/3)$

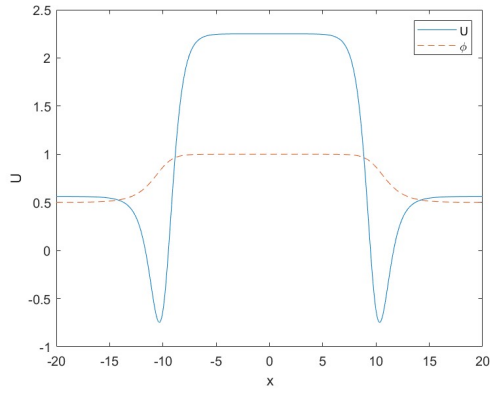
Figure 28 shows that the plots in this topological sector are similar to those in the sector $(-1, -1/3)$. The critical velocity in this sector is $v_c \approx 0.289$. The potential $U(x)$ for the $K\bar{K}$ is of separated double-well, and the raised plateau between two wells is convex. Although the double-well potentials are similar, the phenomena in sector $(-1/3, 1/3)$ are quite different from those in topological sector $(-1/2, 1/2)$. In Figure 29, the left panel shows the $v_{in} - v_{out}$ plot for the two and three bounces. The central panel shows the $v_{in} - v_{out}$ plot for the three and four bounces. The right panel shows the $v_{in} - v_{out}$ plot for the four and five bounces. The v_{in} in the right panel is a zoomed regime in the central



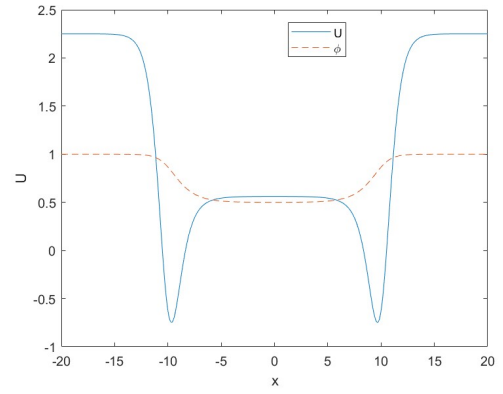
(a) $v_{in} - t$ plot



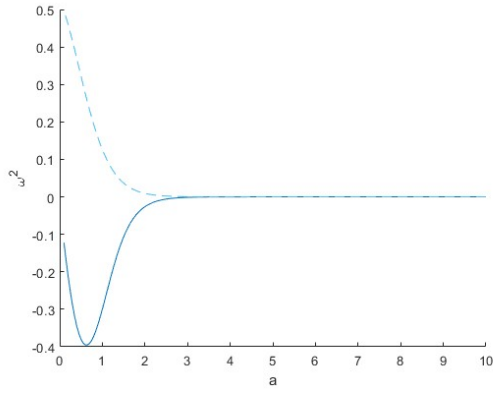
(b) $v_{in} - v_{out}$ plot



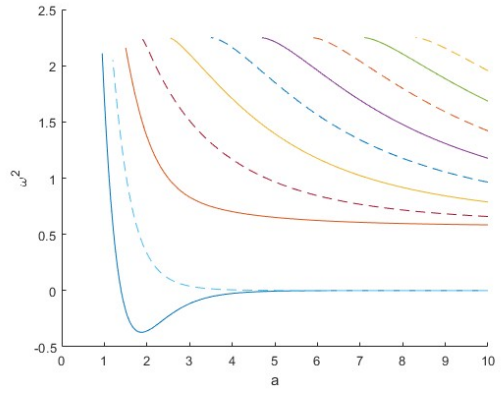
(c) $K\bar{K}$ pair potential $U(x)$ plot



(d) $\bar{K}K$ pair potential $U(x)$ plot

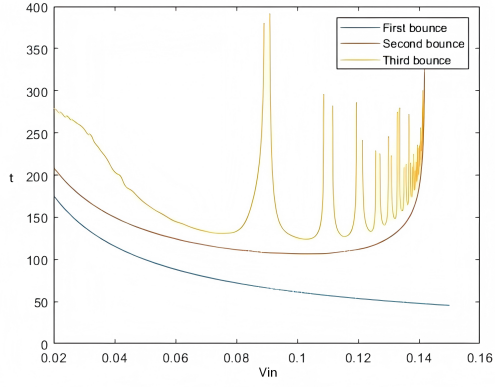


(e) $K\bar{K}$ pair spectrum

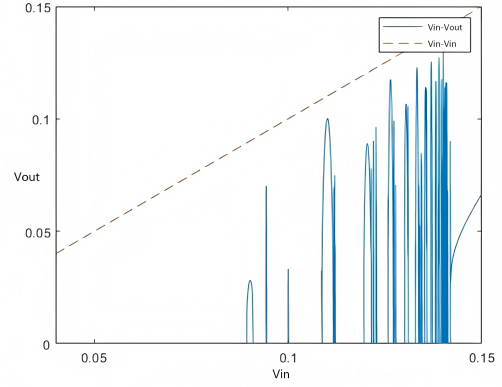


(f) $\bar{K}K$ pair spectrum

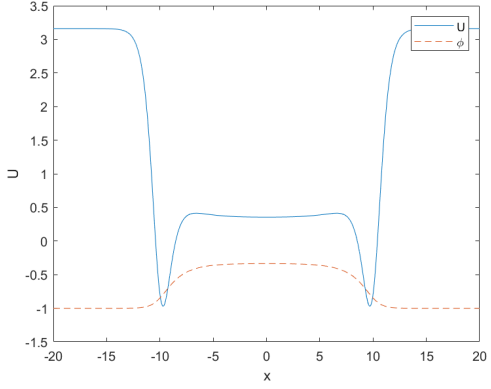
Figure 25: Topological sector $(1/2, 1)$



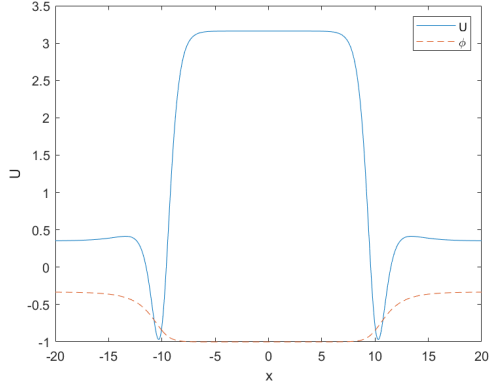
(a) $v_{in} - t$ plot



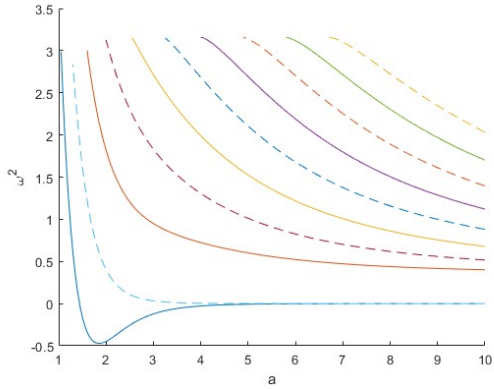
(b) $v_{in} - v_{out}$ plot



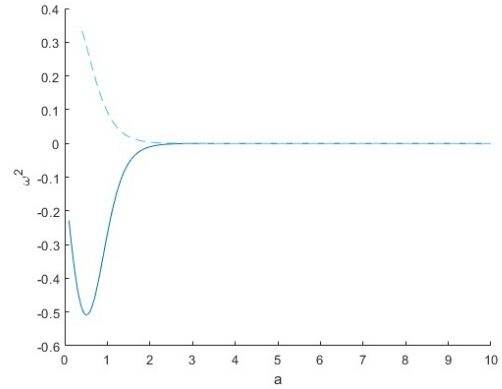
(c) $K\bar{K}$ pair potential $U(x)$ plot



(d) $\bar{K}K$ pair potential $U(x)$ plot



(e) $K\bar{K}$ spectrum



(f) $\bar{K}K$ pair spectrum

Figure 26: Topological sector $(-1, -1/3)$

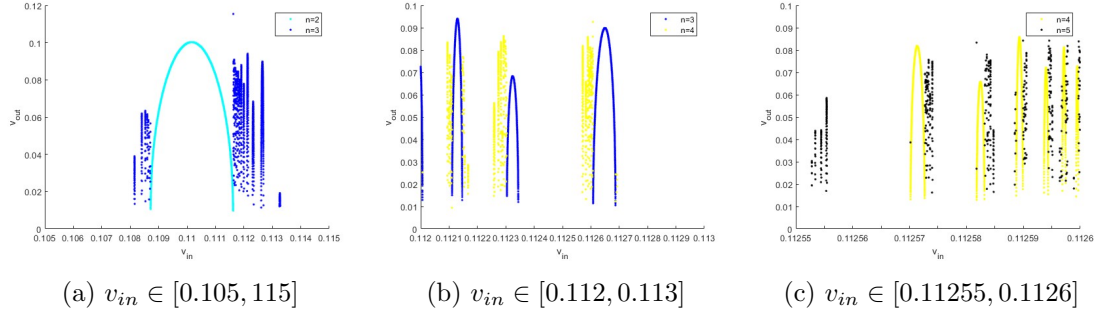
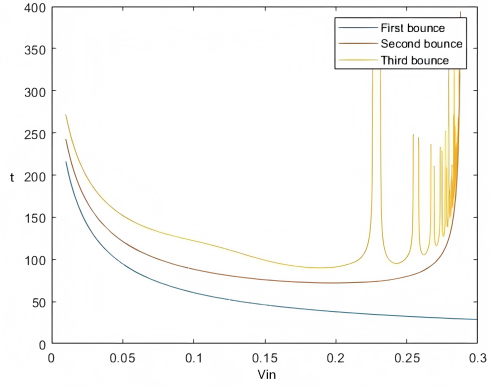


Figure 27: Fractal structure for topological sector $(-1, -1/3)$

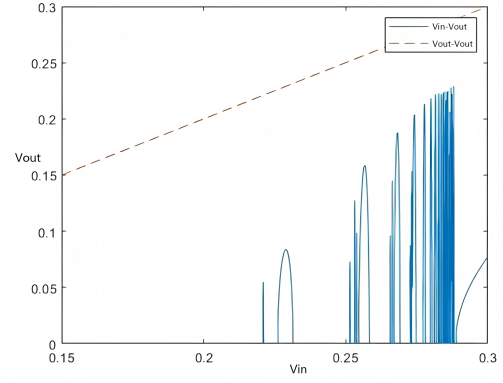
panel, and the v_{in} in the central panel is a zoomed regime in the right panel. This shows the self-similar fractal structure for the soliton collisions.

(iii) *Topological sector $(1/3, 1)$*

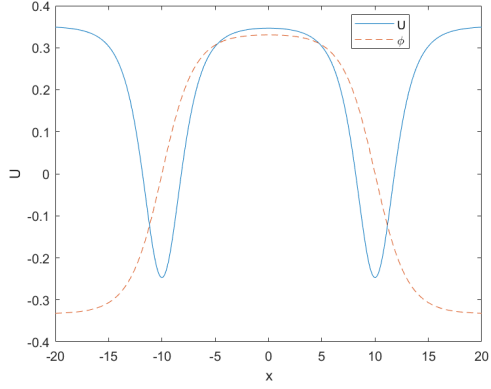
As shown in Figure 16 and Figure 17 of Section 4.1, $K\bar{K}$ pair in this sector always changes sector after collision. No fractal structure exists. Figure 30 reveals that the potential $U(x)$ of $K\bar{K}$ pair has a raised central plateau, while the potential $U(x)$ for the $\bar{K}K$ pair shows a central well. The collision phenomena for the $\bar{K}K$ in the sector $(1/3, 1)$ are the same for the $K\bar{K}$ in the sector $(-1, -1/3)$, and their potentials $U(x)$ are the same.



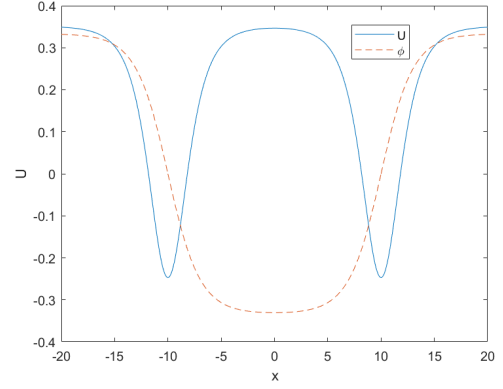
(a) $v_{in} - t$ plot



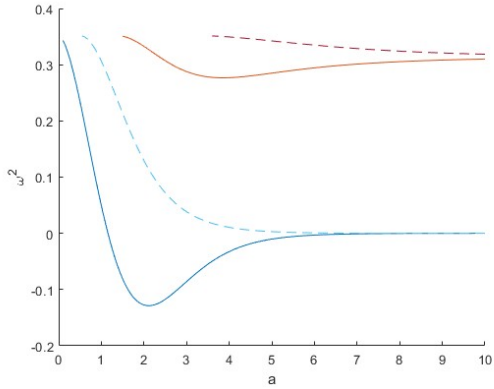
(b) $v_{in} - v_{out}$ plot



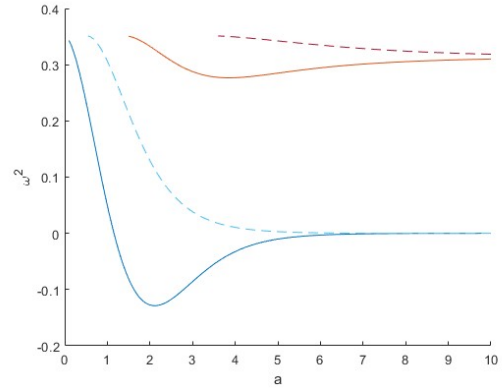
(c) $K\bar{K}$ pair potential $U(x)$ plot



(d) $\bar{K}K$ pair potential $U(x)$ plot



(e) $K\bar{K}$ pair spectrum



(f) $\bar{K}K$ pair spectrum

Figure 28: Topological sector $(-1/3, 1/3)$

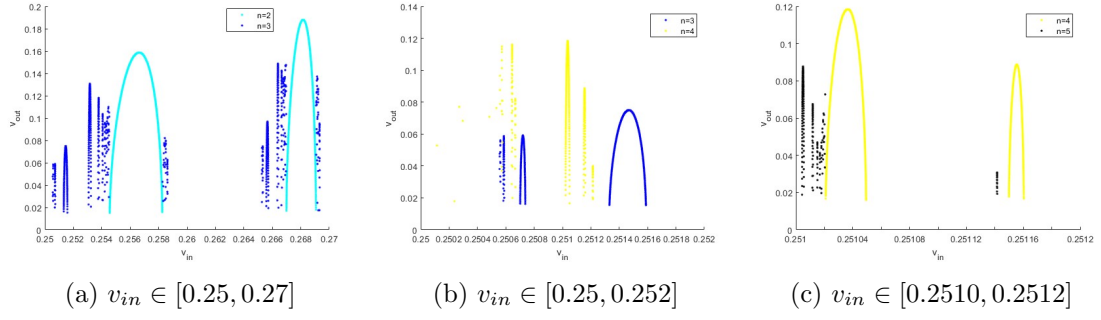


Figure 29: Fractal structure for topological sector $(-1/3, 1/3)$

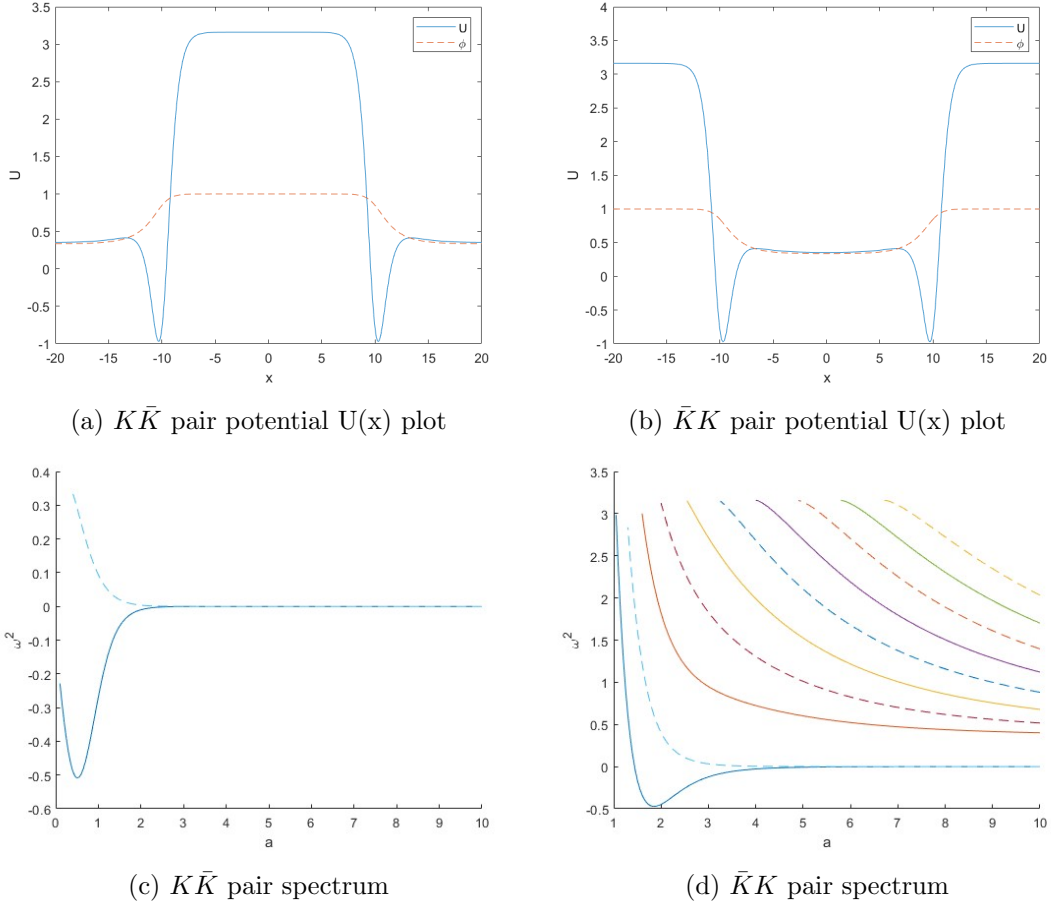


Figure 30: Topological sector $(1/3, 1)$

Table 1: Collection of soliton pairs

Sector	Pair Order	Potential	Bion State	Escape	Annihilation	Changing Sector
$(-1, -1/2)$	$K\bar{K}$	Type I	Yes	Yes	No	No
$(-1, -1/2)$	$\bar{K}K$	Type IIA	Yes	Yes	Yes	No
$(-1/2, 1/2)$	$K\bar{K}$	Type III	No	No	Yes	No
$(-1/2, 1/2)$	$\bar{K}K$	Type III	No	No	Yes	No
$(1/2, 1)$	$K\bar{K}$	Type IIA	Yes	Yes	Yes	No
$(1/2, 1)$	$\bar{K}K$	Type I	Yes	Yes	No	No
$(-1, -1/3)$	$K\bar{K}$	Type I	Yes	Yes	No	No
$(-1, -1/3)$	$\bar{K}K$	Type IIB	No	No	No	Yes
$(-1/3, 1/3)$	$K\bar{K}$	Type IV	Yes	Yes	No	No
$(-1/3, 1/3)$	$\bar{K}K$	Type IV	Yes	Yes	No	No
$(1/3, 1)$	$K\bar{K}$	Type IIB	No	No	No	Yes
$(1/3, 1)$	$\bar{K}K$	Type I	Yes	Yes	No	No

4.3 Unified picture

In Table 1, we summarized the potentials and collision phenomena for all topological sectors. We classify the potentials into five categories, namely Type I, IIA, IIB, III, and IV, respectively. Type I is of central well. Type IIA is of raised central plateau plus a Morse potential on both sides. Type IIB is of raised central plateau plus a modified Morse potential. Type III is of separated double-well with a concave plateau. Type IV is of separated double-well with a convex plateau. From this table, or the collision phenomena, we observe that the potential pattern controls the collision phenomena. Under the same potential, the different soliton pairs have the same collision phenomena, and their spectrum shows the similarity.

We also notice that, when the two solitons collides at center $x = 0$, solitons may pass each other. At this moment, their sector and potential type could change suddenly. This could explain the annihilation and changing sector phenomena. For example, $K\bar{K}$ pair collides in the topological sector $(1/2, 1)$, and then $\phi_{K\bar{K}}$ changes from $(1/2, 1, 1/2)$ to $(1/2, 1/2, 1/2)$. Thus, potential $U = dV/d\phi$ equals 0 for $\phi = constant$. There is no soliton pair solution, which leads the annihilation. In another case, $K\bar{K}$ pair collides in the topological sector $(1/3, 1)$. After solitons passing each other, $\phi_{K\bar{K}}$ changes from $(1/3, 1, 1/3)$ to $(1/3, -1/3, 1/3)$. Thus, potential U changes from Type IIB to Type IV suddenly, leading to a new soliton pair in sector $(-1/3, 1/3)$. Because the new soliton pair always has outgoing velocity exceeding 0.3, solitons always escape and there is no bion state.

5 Conclusion

We have presented a detailed numerical investigation of kink-antikink collisions in a $(1+1)$ -dimensional ϕ^8 scalar field theory. Building on the ϕ^8 model introduced by Gani et al. [13, 18], we derived explicit soliton solutions for different ratios $n = p_2/p_1$, focusing on the cases $n = 2$ and $n = 3$, which possess four distinct degenerate vacua. General boundary conditions and soliton solutions for arbitrary n were also provided.

We implemented numerical methods capable of handling implicit soliton solutions and performed systematic simulations across all topological sectors. Our simulations revealed a rich diversity of collision phenomena, including escape, bion formation, sector transitions, and annihilation. We computed the effective potential and fluctuation spectrum for soliton pairs in specific topological sectors and established a classification scheme that unifies the observed collision phenomenology.

Our work reveals several novel features of the ϕ^8 model that are absent in lower-order theories such as ϕ^4 :

First, we discovered a complete annihilation regime for the $\bar{K}K$ pair in the topological sector $(-1/2, 1/2)$, where annihilation occurs for all initial velocities—a phenomenon not previously reported in ϕ^8 models.

Second, we systematically mapped the fractal structure of resonance windows in multiple sectors, including $(-1, -1/2)$, $(-1, -1/3)$, and $(-1/3, 1/3)$, extending previous illustrative studies to a comprehensive multi-sector cartography.

Third, we demonstrated that the effective potential provides a unified framework for understanding collision outcomes. Crucially, we identified abrupt changes in the potential profile when soliton pairs pass through each other, which explain both the sector-change and annihilation phenomena.

Furthermore, by interchanging the ordering of the kink and antikink within the same topological sector, we showed that the resulting change in the interaction potential is accompanied by corresponding changes in the spectrum, the fractal structure, and the collision outcomes, providing a controlled test of the potential-based classification.

These results establish the ϕ^8 model as a fertile ground for exploring the interplay between topological structure, internal modes, and nonlinear dynamics in field theory.

References

- [1] Nicholas Manton and Paul Sutcliffe. *Topological Solitons*. Cambridge University Press, 2004. DOI: [10.1017/CB09780511617034](https://doi.org/10.1017/CB09780511617034).
- [2] A. R. Bishop, J. A. Krumhansl, and S. E. Trullinger. “Solitons in Condensed Matter: A Paradigm”. In: *Physica D: Nonlinear Phenomena* 1.1 (1980), pp. 1–44. DOI: [10.1016/0167-2789\(80\)90003-2](https://doi.org/10.1016/0167-2789(80)90003-2).
- [3] *Solitons and Condensed Matter Physics: Proceedings of the Symposium on Nonlinear (Soliton) Structure and Dynamics in Condensed Matter* (Oxford, England, June 27–29, 1978). Springer Science & Business Media, 2012.
- [4] Yakov M. Shnir. *Topological and Non-topological Solitons in Scalar Field Theories*. Cambridge University Press, 2018.
- [5] Alexander Vilenkin and E. P. S. Shellard. *Cosmic Strings and Other Topological Defects*. Cambridge University Press, 1994.
- [6] Nicholas S. Manton, Katarzyna Oleś, and Tomasz Romańczukiewicz. “Kink Moduli Spaces: Collective Coordinates Reconsidered”. In: *Physical Review D* 103.2 (2021), p. 025024. DOI: [10.1103/PhysRevD.103.025024](https://doi.org/10.1103/PhysRevD.103.025024).
- [7] Ekaterina Belendryasova and Vakhid A. Gani. “Scattering of the ϕ^8 Kinks with Power-Law Asymptotics”. In: *Communications in Nonlinear Science and Numerical Simulation* 67 (2019), pp. 414–426. DOI: [10.1016/j.cnsns.2018.07.030](https://doi.org/10.1016/j.cnsns.2018.07.030).
- [8] Patrick Dorey, Kieron Mersh, and Tomasz Romančukiewicz. “Kink-Antikink Collisions in the ϕ^6 Model”. In: *Physical Review Letters* 107.9 (2011), p. 091602. DOI: [10.1103/PhysRevLett.107.091602](https://doi.org/10.1103/PhysRevLett.107.091602).
- [9] R. H. Goodman and R. Haberman. “Kink-Antikink Collisions in the ϕ^4 Equation: The n -bounce Resonance and the Separatrix Map”. In: *SIAM Journal on Applied Dynamical Systems* 4.4 (2005), pp. 1195–1228.
- [10] Nicholas S. Manton, Katarzyna Oleś, and Tomasz Romančukiewicz. “Collective Coordinate Model of Kink-Antikink Collisions in ϕ^4 Theory”. In: *Physical Review Letters* 127.7 (2021), p. 071601. DOI: [10.1103/PhysRevLett.127.071601](https://doi.org/10.1103/PhysRevLett.127.071601).
- [11] D. K. Campbell, J. F. Schonfeld, and C. A. Wingate. “Resonance Structure in Kink-Antikink Interactions in ϕ^4 Theory”. In: *Physica D: Nonlinear Phenomena* 9.1-2 (1983), pp. 1–32.
- [12] Vakhid A. Gani, Ali Moradi Marjaneh, and Petr A. Blinov. “Explicit Kinks in Higher-Order Field Theories”. In: *Physical Review D* 101.12 (2020), p. 125017. DOI: [10.1103/PhysRevD.101.125017](https://doi.org/10.1103/PhysRevD.101.125017).
- [13] D. Bazeia, J. G. F. Campos, and A. Mohammadi. “Kink-Antikink Collisions in the ϕ^8 Model: Short-Range to Long-Range Journey”. In: *JHEP* 15.7 (2023), p. 1398. DOI: [10.1007/JHEP05\(2023\)116](https://doi.org/10.1007/JHEP05(2023)116).

- [14] Vakhid A. Gani, A. E. Kudryavtsev, and M. A. Lizunova. “Kink Interactions in the $(1 + 1)$ -Dimensional ϕ^6 Model”. In: *Physical Review D* 89.12 (2014), p. 125009. DOI: [10.1103/PhysRevD.89.125009](https://doi.org/10.1103/PhysRevD.89.125009).
- [15] M. K. Prasad and C. M. Sommerfield. “Exact Classical Solution for the ’t Hooft Monopole and the Julia-Zee Dyon”. In: *Physical Review Letters* 35.12 (1975), p. 760. DOI: [10.1103/PhysRevLett.35.760](https://doi.org/10.1103/PhysRevLett.35.760).
- [16] Mariya Lizunova and Jasper Van Wezel. “An Introduction to Kinks in φ^4 -Theory”. In: *SciPost Physics Lecture Notes* (2021), p. 023. DOI: [10.21468/SciPostPhysLectNotes.23](https://doi.org/10.21468/SciPostPhysLectNotes.23).
- [17] Milad Mohammadi and Emad Momeni. “Scattering of Kinks in the $B\phi^4$ Model”. In: *Chaos, Solitons & Fractals* 163 (2022), p. 112834. DOI: [10.1016/j.chaos.2022.112834](https://doi.org/10.1016/j.chaos.2022.112834).
- [18] Ivan C. Christov et al. “Kink-antikink collisions and multi-bounce resonance windows in higher-order field theories”. In: *Communications in Nonlinear Science and Numerical Simulation* 97 (2021), p. 105748.
- [19] João G. F. Campos and Azadeh Mohammadi. “Kink-antikink collision in the supersymmetric ϕ^4 model”. In: *Journal of High Energy Physics* 2022.8 (Aug. 2022), p. 180. DOI: [10.1007/JHEP08\(2022\)180](https://doi.org/10.1007/JHEP08(2022)180).
- [20] Aslihan Demirkaya et al. “Kink dynamics in a parametric ϕ^6 system: a model with controllably many internal modes”. In: *Journal of High Energy Physics* 2017.12 (Dec. 2017), p. 071. DOI: [10.1007/JHEP12\(2017\)071](https://doi.org/10.1007/JHEP12(2017)071).
- [21] Anupam Das, Suman Kar, and Subhrajit Samanta. “Resonance Structures in Kink-Antikink Scattering in a Quantum Vacuum”. In: *Physical Review D* 107.11 (2023), p. 116017. DOI: [10.1103/PhysRevD.107.116017](https://doi.org/10.1103/PhysRevD.107.116017).
- [22] S. K. Sahu and P. K. Panigrahi. “Scattering of Kinks in Noncanonical Sine-Gordon Model”. In: *Turk. J. Phys* 2023.3 (2023), p. 187.
- [23] G. Dattoli, A. Torre, and F. Bajardi. “Kink-Antikink Scattering-Induced Breathing Bound States and Oscillons in a Parametrized ϕ^4 Model”. In: *Annals Phys* 96.5 (2021), p. 055202. DOI: [10.1142/S0217732321500152](https://doi.org/10.1142/S0217732321500152).